Viscous extension of potential-flow unsteady aerodynamics: the lift frequency response problem

Haithem Taha[1,†] and Amir S. Rezaei[1]

[1]Mechanical and Aerospace Engineering, University of California, Irvine, CA 92697, USA

The application of the Kutta condition to unsteady flows has been controversial over the years, with increased research activities over the 1970s and 1980s. This dissatisfaction with the Kutta condition has been recently rejuvenated with the increased interest in low-Reynolds-number, high-frequency bio-inspired flight. However, there is no convincing alternative to the Kutta condition, even though it is not mathematically derived. Realizing that the lift generation and vorticity production are essentially viscous processes, we provide a viscous extension of the classical theory of unsteady aerodynamics by relaxing the Kutta condition. We introduce a trailing-edge singularity term in the pressure distribution and determine its strength by using the triple-deck viscous boundary layer theory. Based on the extended theory, we develop (for the first time) a theoretical viscous (Reynolds-number-dependent) extension of the Theodorsen lift frequency response function. It is found that viscosity induces more phase lag to the Theodorsen function particularly at high frequencies and low Reynolds numbers. The obtained theoretical results are validated against numerical laminar simulations of Navier–Stokes equations over a sinusoidally pitching NACA 0012 at low Reynolds numbers and using Reynolds-averaged Navier–Stokes equations at relatively high Reynolds numbers. The physics behind the observed viscosity-induced lag is discussed in relation to wake viscous damping, circulation development and the Kutta condition. Also, the viscous contribution to the lift is shown to significantly decrease the virtual mass, particularly at high frequencies and Reynolds numbers.

Key words: boundary layer structure, low-dimensional model, wakes

1. Introduction

Recalling the historical development of the classical theory of unsteady aerodynamics (unsteady aerodynamics of wings in an incompressible flow), we realize that it is mainly based on the following fundamental assumption due to Prandtl (1924) and Birnbaum (1924): for a high-Reynolds-number, small-angle-of-attack flow around an infinitely thin airfoil, separation or sheets of vorticity are shed from the sharp edges only and the flow outside of these sheets can be considered irrotational.

† Email address for correspondence: hetaha@uci.edu

This brilliant assumption is quite accurate in the stated regime and was extremely enabling. Because an incompressible irrotational flow is simply governed by the Laplace equation, which is a linear equation admitting superposition, this framework was the basis for almost all analytical theories of aerodynamics in the linear regime: the steady ones such as the thin airfoil theory (Birnbaum & Ackermann 1923; Glauert 1926), Prandtl's lifting line theory (Prandtl 1918), Weissinger's extended lifting line theory (Weissinger 1949) and the lifting surface theory (Multhopp 1950; Truckenbrodt 1953), which evolved into the vortex lattice/panel method; and the unsteady ones such as Theodorsen's lift frequency response (Theodorsen 1935), Wagner's lift step response (Wagner 1925), Kussner's sharp-edged gust problem (Küssner 1929) and the developments of Von Karman & Sears (1938), among others. In addition, it still acts as the pillar of many recent developments (Jones 2003; Yongliang, Binggang & Huiyang 2003; Pullin & Wang 2004; Ansari, Żbikowski & Knowles 2006*a*; Michelin & Smith 2009; Tchieu & Leonard 2011; Ramesh *et al.* 2013; Wang & Eldredge 2013; Ramesh *et al.* 2014; Taha, Hajj & Beran 2014; Yan, Taha & Hajj 2014; Li & Wu 2015; Xia & Mohseni 2017; Hussein *et al.* 2018). However, this framework using potential flow is not complete and requires a closure or auxiliary condition (e.g. the Kutta condition). In particular, it does not provide how much vorticity is shed at the sharp trailing edge. This quantity is essential, as it immediately determines the circulation over the airfoil through conservation of circulation, which in turn dictates the lift via the Kutta–Joukowsky lift theorem (Kutta 1902; Joukowsky 1910). Therefore, the potential-flow theory alone cannot predict the generated lift force. However, if the potential-flow theory is supplied with the generated lift force, it will provide a reasonable (sometimes accurate) representation of the flow field even in unsteady high-angle-of-attack situations, as shown in the recent efforts of Pitt Ford & Babinsky (2013) and Hemati, Eldredge & Speyer (2014). They basically showed that by using the 'right' auxiliary condition to determine the circulation development over the airfoil, the resulting potential-flow field is quite close to the actual flow field even at unsteady high-angle-of-attack situations where vortices also shed from the leading edge. We interpret these results from a dynamical system perspective as an observability result: the flow dynamics are observable from the lift force (or circulation) output measurement and the observer (a reduced-order observer) is given by the potential-flow dynamics. That is, given the generated aerodynamic forces, one can estimate (observe) the flow dynamical states (e.g. the velocity field). However, the generated aerodynamic forces are the primary unknowns of interest to an aerodynamicist.

The most common auxiliary condition that has typically been used throughout the history of potential-flow aerodynamics is the Kutta condition. It completes the potential-flow framework by providing the circulation around the airfoil (equivalently the generated lift force). It has several representations: smooth flow off the trailing edge, no flow around the trailing edge, or that the stagnation point is right at the trailing edge, among other forms. It is quite accurate for a steady flow (at high Reynolds number and small angle of attack) as can be seen from Prandtl's flow visualizations in his water channel early in the last century. Figure 1(*b*) shows smooth flow off the trailing edge and that there is no flow around the trailing edge from the lower surface to the upper surface or *vice versa*; that is, the stagnation point is at the trailing edge and the Kutta condition is essentially satisfied. Indeed, it is a paradigm for engineering ingenuity where a mathematical condition is inferred from physical observations. However, for an unsteady case such as the one shown in figure 1(*a*), it is already known that, in the early transient moments after an
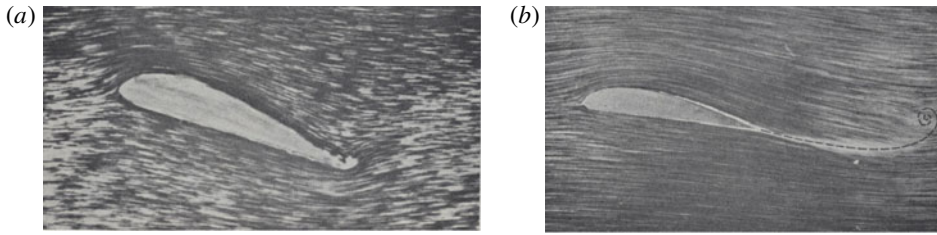
FIGURE 1. Visualization of the impulsive start flow around an airfoil (Tietjens & Prandtl 1934, pp. 296–299): (*a*) early transient; (*b*) steady state. During the transient period, the flow rotates around the trailing edge. After reaching steady state, the flow leaves the trailing edge smoothly and the Kutta condition is satisfied.

impulsive start, the flow goes around the trailing edge from the lower surface to the upper surface and the stagnation point is on the upper surface (Tietjens & Prandtl 1934, pp. 158–168; Goldstein 1938, pp. 26–36; Schlichting & Truckenbrodt 1979, pp. 33–35).

The application of the Kutta condition to unsteady flows has been controversial. The reader is referred to the articles by Sears (1956, 1976) and the review article on the topic by Crighton (1985), although, the latter's definition of the Kutta condition is different from the current discussion or that by Sears. Crighton defined the Kutta condition as a condition of least singularity at the edge, which may even come from viscous considerations (i.e. boundary layer theory). However, in this case, we (similar to Sears' viewpoint) would consider it as a viscous extension of the Kutta condition. The need for an auxiliary condition alternative to Kutta's goes back as early as the work of Howarth (1935); the research efforts on the applicability of the Kutta condition to unsteady flows reached its peak in the 1970s and 1980s (Basu & Hancock 1978; Daniels 1978; Satyanarayana & Davis 1978; Bass, Johnson & Unruh 1982; Crighton 1985). This research was partly motivated by the failure to capture an accurate flutter boundary (Rott & George 1955; Abramson & Chu 1959; Henry 1961; Abramson & Ransleben 1965). Recall that the flutter phenomenon is simply an interaction between unsteady aerodynamics and structural dynamics. In addition, since structural dynamics could be captured with a good accuracy (e.g. exact beam theory), it has been deemed that the flaw stems from the classical unsteady aerodynamic theory, particularly the Kutta condition, as suggested by Chu (1961) and Shen & Crimi (1965) among others. Moreover, since these deviations occurred even at zero angle of attack or lift (Woolston & Castile 1951; Chu & Abramson 1959), it was inferred that there is a fundamental issue with such a theory that is not merely a higher-order nonlinear effect (Chu 1961). Therefore, there was almost a consensus that the Kutta condition has to be relaxed particularly at large frequencies, large angles of attack and/or low Reynolds numbers (Abramson, Chu & Irick 1967; Satyanarayana & Davis 1978; Savage, Newman & Wong 1979). In fact, Orszag & Crow (1970) regarded the full-Kutta-condition solution as 'indefensible'.

Interestingly, this dissatisfaction with the Kutta condition and the need for its relaxation has recently been rejuvenated. Several recent efforts invoked an alternative auxiliary condition to Kutta's. Ansari *et al.* (2006*a*) and Ansari, Żbikowski & Knowles (2006*b*) asked for a modified version of the Kutta condition, particularly during rapid pitching near stroke reversals, to avoid creating artificially strong vortices; the manoeuvre is so acute that the fluid may actually flow around the edge not along it.

More recently, Pitt Ford & Babinsky (2013) experimentally studied the leading-edge vortex (LEV) dynamics over an impulsively started flat plate. They also developed a potential-flow model that consists of a bound circulation, free LEVs and free trailing-edge vortices. They determined the positions and strengths of the vortices by applying the γ_2 method (Graftieaux, Michard & Grosjean 2001) to their particle image velocimetry (PIV) measurements. Based on these values, they determined the value of the bound circulation that minimizes the deviation between the potential-flow field and PIV measurements. During early stages, the optimum bound circulation was found to be considerably different from the Kutta's value (which ensures finite velocity at the trailing edge). In a similar setting, Hemati *et al.* (2014) improved their previous varying-strength discrete vortex model (Wang & Eldredge 2013) by relaxing the Kutta condition via applying optimal control theory to determine the strengths of the recently shed vortices that minimize the discrepancy between the potential-flow predicted forces and measurements, which was also found to be considerably different from Kutta's values.

Ramesh *et al.* (2014) developed a new LEV shedding criterion based on the first (singular) term in the well-known Fourier series representation of the bound circulation distribution in the classical thin airfoil theory. This term, which they called the leading-edge suction parameter (LESP), is a measure of leading-edge suction (Garrick 1937). Ramesh *et al.* (2014) showed that there is a critical value of the LESP (depending on airfoil shape and Reynolds number) that determines whether the flow is attached or separated at the leading edge, irrespective of the motion kinematics. Their LESP criterion predicts not only the onset and termination of LEV shedding but also the strength of the newly shed LEV, thereby removing the need for an auxiliary condition at the leading edge. Nevertheless, they applied the Kutta condition at the trailing edge. It is also noteworthy to mention the recent efforts of Xia & Mohseni (2017) who extended Jones's (2003) auxiliary condition at the sharp edges of a flat plate to the case of a finite trailing-edge angle. Jones (2003) used the Rott–Birkhoff equation (Rott 1956; Birkhoff 1962) to model the dynamics of free continuous vortex sheets emanating from the leading and trailing edges. He satisfied the Kutta condition at both edges by imposing boundedness of the flow velocity everywhere. This formulation led to the edge condition: the vortex sheet sheds tangentially to the plate. However, this result is applicable only to a flat plate or an airfoil with cusped trailing edge. Xia & Mohseni (2017) extended it to the case of an airfoil with finite trailing-edge angle by requiring that the flow velocity be tangential to the vortex sheet at the edge. Using this condition, together with conservation of momentum, Xia & Mohseni (2017) derived two equations that generalize Jones's edge condition (governing the shedding of a continuous vortex sheet from a sharp edge with zero angle) to the case of a finite edge angle.

Indeed, the development of an auxiliary condition that replaces the Kutta condition in highly unsteady flows is a pressing issue that has persisted over almost a century. Since the vorticity generation and lift development are essentially viscous processes, a purely inviscid theory of unsteady aerodynamics might be fundamentally flawed. Here, we develop a viscous extension of the classical theory of unsteady aerodynamics: equivalently an unsteady extension of the viscous boundary layer theory. In particular, we revisit the unsteady boundary layer triple-deck theory developed by Brown & Daniels (1975) and Brown & Cheng (1981) to develop a viscous extension of Theodorsen's lift frequency response. In §3, we extend their effort (on a flat plate pitching around its mid-chord point) to the more general case of an arbitrarily deforming thin airfoil (or time-varying camber), while correcting for a few minor

mistakes. In §4, using a describing function formulation, we develop for the first time a viscous (Reynolds-number-dependent) lift frequency response. In §5, we perform a computational simulation using ANSYS Fluent for a harmonically pitching airfoil (NACA 0012) to assess the validity of the obtained results from the unsteady triple-deck theory. Finally, we provide in §6 a physical explanation of the obtained results, namely a discussion on the relation between the viscosity-induced lag in circulation development and the Kutta condition.

2. The triple-deck boundary layer theory

During his PhD study under Prandtl, Blasius (1908) solved Prandtl's boundary layer equations subject to a no-slip boundary condition on a flat plate. Via similarity transformation, he obtained the celebrated Blasius solution resulting in a boundary layer thickness of order $R^{-1/2}$, where R is the Reynolds number based on the plate chord length. Later, Goldstein (1930) solved exactly the same equations subject to a different boundary condition: zero stress on the wake centreline behind the flat plate. His solution for the stream function near the edge constituted of a Blasius function at the edge plus corrections in the form of $x^{1/3}$, where x is the distance downstream of the trailing edge. As such, Goldstein's solution is not uniformly valid as $x \to 0$: the transverse velocity has a singularity at $x = 0$. Moreover, when taking into account the effect of Goldstein's boundary layer on the outside potential flow, it induces an adverse pressure gradient upstream of the edge (above the Blasius layer) and a favourable pressure gradient downstream of the edge (Messiter 1970). That is, the removal of the plate's surface accelerates the flow behind the plate, leading to a favourable pressure gradient. Therefore, in the vicinity of the trailing edge, there are two boundary layers interacting with each other. It is expected that neither Blasius nor Goldstein solution is valid in the immediate vicinity of the edge where the x derivatives become large due to the abrupt change in the viscous boundary condition. The triple-deck theory has been originally devised to model these local interactions near the trailing edge of an airfoil in steady flow due to the transition from a modified Blasius boundary layer with an adverse pressure gradient to a modified Goldstein near-wake solution with a favourable pressure gradient (Crighton 1985). In other words, the triple-deck structure represents a solution to the discontinuity of the viscous boundary condition at the edge (Brown & Daniels 1975): from a zero tangential velocity on the airfoil to a zero pressure discontinuity on the wake centreline. As shown in figure 2, this interaction typically takes place over a short length of order $R^{-3/8}$, similar to Lighthill's supersonic shock wave–boundary layer interaction (Lighthill 1953). Over this range, the correction in the boundary layer solution due to the non-zero pressure gradient becomes of the same order as the leading term (Messiter 1970). Therefore, unlike the typical boundary layer theory where scaling (zooming) is applied to the y-axis only, the x-axis is also scaled in the triple-deck theory to discern the details of such a transition. As shown in figure 2, aerodynamicists modelled this transition through three decks (triple-deck theory): (i) the upper deck which comprises an irrotational flow outside of the main boundary layer; (ii) the main deck which comprises a Blasius-like layer, though it becomes inviscid; and (iii) the lower deck, which is a sublayer inside the main boundary layer where the nonlinear boundary layer equations are applied and the viscous boundary condition must be satisfied. For more details, the reader is referred to the review articles by Stewartson (1974, 1981), Messiter (1983), Smith (1983) and Crighton (1985) and the references therein.
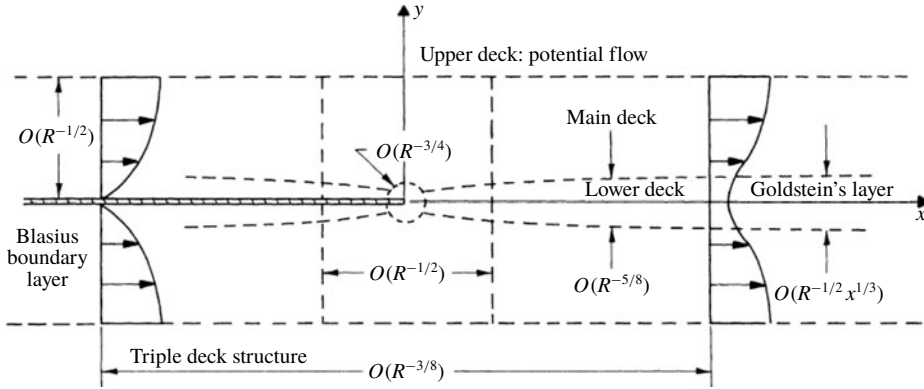
FIGURE 2. Triple-deck structure and various flow regimes; adapted from Messiter (1970).

One of the useful outcomes from the triple-deck theory is its correction to the Blasius skin friction drag $C_D \simeq 1.328/\sqrt{R}$, which is valid only for high enough Reynolds number. However, the triple-deck extension

$$C_D \simeq \frac{1.328}{\sqrt{R}} + \frac{2.66}{R^{7/8}} \qquad (2.1)$$

of the Blasius skin friction drag coefficient is in very good agreement with both Navier–Stokes simulations and experiments down to $R = 10$ and even lower (Crighton 1985). Another useful outcome from the triple-deck theory, which is one stepping stone to the theory developed in this work, is the trailing-edge stall concept and the viscous correction of the steady pressure distribution. This result is discussed next.

Stewartson (1968) and Messiter (1970) were the first to develop the triple-deck theory for a flat plate in a steady flow at zero angle of attack. Brown & Stewartson (1970) extended such work to a non-zero angle of attack in the order of $R^{-1/16}$. Over this range, the resulting adverse pressure gradient is of the same order as the favourable pressure gradient in the triple deck, leading to separation in the immediate vicinity of the trailing edge, which is called trailing-edge stall. To provide a viscous correction for the steady Kutta–Joukowsky lift, Brown & Stewartson (1970) introduced a deviation from the Kutta circulation, which will cause a singularity in the loading at the trailing edge.

Consider a flat plate with a semi-chord length b subject to a steady uniform flow U at an angle of attack α_s. Let $\tilde{x}$ be the plate coordinate normalized by b (i.e. $-1 \leqslant \tilde{x} \leqslant 1$ over the plate). The potential-flow velocity distribution on the upper surface of the plate can be written as

$$\frac{u}{U} = 1 + \alpha_s \sqrt{\frac{1 - \tilde{x}}{1 + \tilde{x}}} - \frac{B_s}{\sqrt{1 - \tilde{x}^2}}. \qquad (2.2)$$

(Equation (2.2) is given as (2.2) by Brown & Stewartson (1970) and rewritten here in the terminology of this paper. In particular, their B is related to our B_s as $B = B_s b/\alpha_s$.) In equation (2.2), B_s is the deviation from the (correction to the) Kutta circulation, which leads to a singularity at the trailing edge (actually both edges); it can be related to the stagnation point as $B_s = \sin\theta_{st}$, where θ_{st} is the angle of the stagnation point in
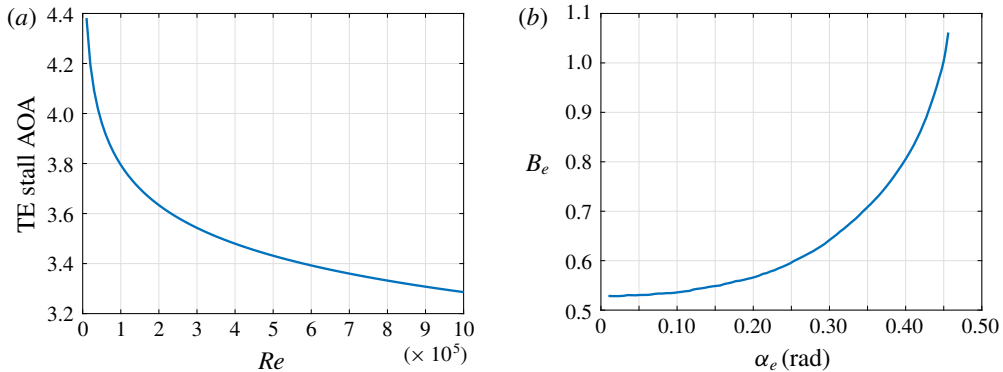
FIGURE 3. (Colour online) Results of the steady triple-deck boundary layer theory. (*a*) Variation of the trailing-edge stall angle of attack (AOA) with Reynolds number. (*b*) Numerical solution of the steady lower-deck equations for $0 < \alpha_e < 0.45$. For panel (*a*), α_e is set to the trailing-edge stall value (0.47) and the corresponding actual angle of attack α_s is determined from (2.4) based on the Reynolds number R. The trailing-edge stall angle of attack decreases as R increases. Panel (*b*) is adapted from Chow & Melnik (1976).

the cylinder domain. There is no means within potential flow to determine the strength B_s of this singularity. The Kutta condition dictates that it must vanish; the stagnation point lies at the trailing edge. In contrast, Brown & Stewartson (1970) proposed to determine the value of B_s (trailing-edge singularity) by matching the triple deck with the outer potential flow. Brown & Stewartson (1970) formulated such a problem and showed that the flow in the lower deck is governed by partial differential equations that are solved numerically for each value of $\alpha_e = R^{1/16}\lambda^{-9/8}\alpha_s$, where $\lambda = 0.332$ is the Blasius skin friction coefficient. Jobe & Burggraf (1974) and Veldmann & Van de Vooren (1975) solved the $\alpha_e = 0$ case, while Chow & Melnik (1976) solved the case of $0 < \alpha_e < 0.45$ and concluded that the flow will separate from the suction side of the airfoil from the trailing edge at $\alpha_e = 0.47$ (trailing-edge stall angle). This result leads to an inverse relation between Reynolds number and the actual trailing-edge stall angle of attack, as shown in figure 3(*a*), which yields quite a small value for the airfoil angle of attack before trailing-edge stall: $\alpha_s = 3.1$–$4.2°$ for $R = 10^4$–10^6.

Applying Bernoulli's equation to (2.2), Chow & Melnik (1976) wrote the steady pressure distribution over the upper surface of the plate near the trailing edge (i.e. $\tilde{x} \to 1$) as

$$P_s(\tilde{x} \to 1) - P_\infty = \rho U^2 \left[-\alpha_s\sqrt{\frac{1-\tilde{x}}{2}} + \frac{B_s/2}{\sqrt{\frac{1-\tilde{x}}{2}}} \right]. \qquad (2.3)$$

(Equation (2.3) is given as (7) by Chow & Melnik (1976) and rewritten here in the terminology of this paper. In particular, their a_1 is written here as B_e, which is related to B_s via (2.4).) In equation (2.3), ρ is the fluid density, P_∞ is the pressure of the undisturbed uniform flow, and the pressure on the lower side is given by the negative of (2.3). The numerical solution by Chow & Melnik (1976) provides the strength B_s of the trailing-edge singularity in terms of the angle of attack α_s in an indirect way: they provided a scaled/equivalent B_s (denoted here by B_e) as a nonlinear function of
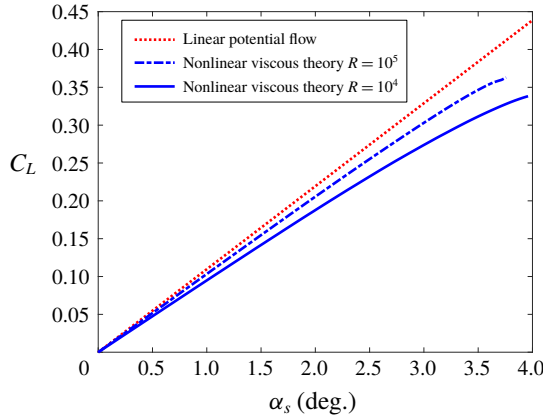
FIGURE 4. (Colour online) Nonlinear steady C_L–α relation from the viscous boundary layer theory. It is constructed based on the steady version of the theory detailed below – equivalently the viscous steady theory of Brown & Stewartson (1970) and the numerical solution of Chow & Melnik (1976). The C_L–α relation becomes more nonlinear as R decreases and there is a lift decrease towards trailing-edge stall.

a scaled/equivalent α_s (denoted here by α_e), which is represented here in figure 3(b), where the scaling is given by

$$\alpha_e = \alpha_s \epsilon^{-1/2} \lambda^{-9/8}, \quad B_s = 2\epsilon^3 \lambda^{-5/4} B_e(\alpha_e) \alpha_s, \tag{2.4a,b}$$

where α_s and α_e are in radians, and $\epsilon = R^{-1/8} \ll 1$ (Stewartson 1968).

Using the velocity distribution (2.2) and Bernoulli's equation, one can determine the steady lift coefficient as

$$C_L = 2\pi(\sin \alpha_s - B_s) = 2\pi(\sin \alpha_s - \sin \theta_{st}). \tag{2.5}$$

Figure 4 shows the nonlinear variation of the steady lift coefficient C_L with the angle of attack α_s up to the trailing-edge stall angle at different Reynolds numbers. Equation (2.5) points to important implications for lift control purposes: controlling the stagnation point has an effect on the lift that is as significant as changing the angle of attack. A $3°$ change in the stagnation point in the cylinder domain has the same effect on the lift as changing the angle of attack by the same amount ($3°$). It should be noted that the former change corresponds to a very slight shift in the stagnation point from the trailing edge in the plate domain: 0.14%.

3. Unsteady triple-deck theory

3.1. *Background and main concept*

Brown & Daniels (1975) were the first to extend the steady triple-deck theory to the case of a high-frequency (ω), small-amplitude oscillatory pitching flat plate. Unlike the steady case, there is a Stokes layer near the wall that is of order $\sqrt{\nu/\omega}$ where the viscous term is balanced by the time-derivative term in the equations. Brown & Daniels assumed that the Stokes layer and the lower deck have the same thickness, which results in a reduced frequency $k = O(R^{1/4})$, where $k = \omega b/U$. This range is too large for engineering applications: $k \simeq 5$–15 for $R = 10^4$–10^6. Then, the matching

between the adverse pressure gradient due to oscillation and the triple-deck favourable pressure gradient results in a pitching amplitude of the order of $O(R^{-9/16})$, which is also impractically small for engineering applications: $\simeq 0.02°$–$0.32°$ for $R = 10^4$–10^6. Indeed, their work is for very-high-frequency, very-small-amplitude oscillations. Note that, over this range, in contrast to the engineering-relevant problem considered in this work, the triple-deck problem becomes mathematically interesting as the time-derivative term appears in the lower-deck equations.

Brown & Cheng (1981) extended the work of Brown & Daniels (1975) to a more practical range of parameters $0 < k \ll R^{1/4}$. They provided a solution for the case of a flat plate pitching about its mid-chord at $k = 1/2$. In this section, we extend their work to an arbitrarily deforming thin airfoil, arbitrary k in the range $0 < k \ll R^{1/4}$, and correct for a few minor mistakes in their derivation. More importantly, we use the developed theory, within a describing function formulation (Krylov & Bogoliubov 1943) assuming weakly nonlinear dynamics, to provide a viscous extension of the classical Theodorsen's lift frequency response, which was not provided by Brown & Cheng (1981).

A key element in the theoretical development below is the vanishing of the time-derivative term from the triple-deck equations over the range $0 < k \ll R^{1/4}$. That is, the lower-deck equations are quite similar to those of the steady case at a non-zero α_s studied by Brown & Stewartson (1970) with a proper definition for the equivalent steady angle of attack. However, we emphasize that this approach is not a quasi-steady solution; although the time-derivative term does not show up in the lower-deck equations, the correspondence with the steady equations implies an equivalent angle of attack that is dependent on the oscillation frequency, as shown below. Therefore, the lower-deck system is dynamical (i.e. possesses a non-trivial frequency response). In fact, even with no time-derivative term in the lower-deck equations, it is not obvious how the steady results of Brown & Stewartson (1970) can be readily applied because the upstream flow is unsteady with Stokes layer in the perturbed Blasius layer. Brown & Daniels (1975) encountered a similar problem: how to match the solution of the perturbed Blasius boundary layer (with its inner Stokes layer) with the main deck of the triple-deck structure? They resolved this issue by introducing a transition region, whose length is $O(k^{-1})$, between the perturbed Blasius boundary layer and the triple deck, called the fore deck. It has similar structure to that upstream of the triple deck: outer potential flow, main boundary layer and an inner Stokes layer, as shown in figure 5. Therefore, in the low-frequency problem where the triple-deck equations are void of the time-derivative term, to match the unsteady flow upstream of the triple deck with the 'quasi-steady' flow in the triple deck, Brown & Cheng (1981) inserted a second fore deck between the first fore deck and the triple deck, as shown in figure 5. As such, the numerical results of Chow & Melnik (1976) to the steady problem of Brown & Stewartson (1970) could be readily used with an equivalent angle of attack. Since the equivalent steady angle of attack α_s is proportional to $A_\alpha k^2$ (where A_α is the amplitude of oscillation), and the steady triple-deck formulation of Brown & Stewartson (1970) is valid for $\alpha_s = O(R^{-1/16})$, the current unsteady formulation is valid for $A_\alpha k^2 = O(R^{-1/16})$, which is quite relevant to engineering applications (e.g. $R \simeq 10^6$, $A_\alpha \simeq 5°$ and $k < 5$).

3.2. *Theoretical development*

3.2.1. *Potential-flow set-up*

Consider an arbitrarily deforming thin airfoil (i.e. of time-varying camber) in the presence of a uniform stream U, as shown in figure 6. In classical thin airfoil theory
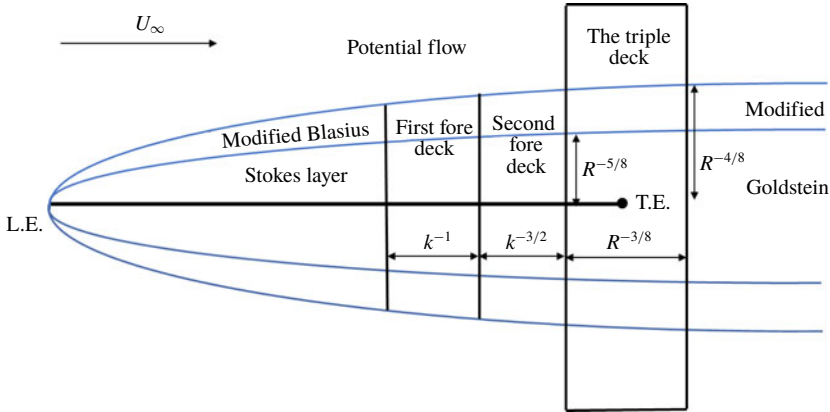
FIGURE 5. (Colour online) Low-frequency triple-deck structure and flow regimes.
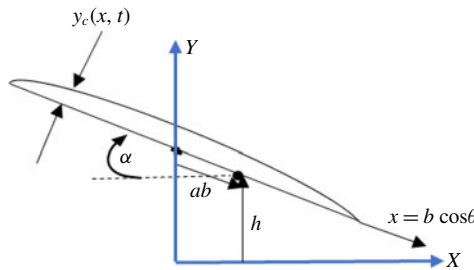

FIGURE 6. (Colour online) A flexible/deformable thin airfoil defined by the time-varying camber function $y_c(x, t)$.

(e.g. Robinson & Laurmann 1956; Schlichting & Truckenbrodt 1979; Bisplinghoff, Ashley & Halfman 1996), it is typical to assume the following series solution for the pressure distribution over the upper surface, which automatically satisfies the Kutta condition (zero loading at the trailing edge):

$$P(\theta, t) - P_\infty = \rho \left[\frac{1}{2} a_0(t) \tan \frac{\theta}{2} + \sum_{n=1}^{\infty} a_n(t) \sin n\theta \right], \qquad (3.1)$$

where θ is related to x via $x = b \cos \theta$ and a_0 represents the leading-edge singularity. The pressure on the lower side is given by the negative of (3.1). Moreover, if the plate's normal velocity v_p is written as

$$v_p(\theta, t) = \frac{1}{2} b_0(t) + \sum_{n=1}^{\infty} b_n(t) \cos n\theta, \qquad (3.2)$$

then the no-penetration boundary condition will provide a means to determine all the coefficients a_n (except a_0) in terms of the plate motion kinematics (b_n) as (Robinson & Laurmann 1956, p. 491)

$$a_n(t) = \frac{b}{2n} \dot{b}_{n-1}(t) + U b_n(t) - \frac{b}{2n} \dot{b}_{n+1}(t), \quad \forall \, n \geqslant 1. \qquad (3.3)$$

The determination of a_0 is more involved in the sense that it requires solving an integral equation, which cannot be solved analytically for arbitrarily time-varying wing motion. It has been solved for some common inputs; e.g. step change in the angle of attack resulting in Wagner's response (Wagner 1925), simple harmonic motion resulting in Theodorsen's frequency response (Theodorsen 1935) and a sharp-edged gust (Küssner 1929). Since the focus of this work is to provide a viscous extension of Theodorsen's frequency response, consider the simple harmonic motion

$$v_p(\theta, t) = V_p(\theta)e^{i\omega t}, \quad V_p(\theta) = \frac{1}{2}B_0 + \sum_{n=1}^{\infty} B_n \cos n\theta, \quad (3.4a,b)$$

where the spatially varying amplitude $V_p(\theta)$ may be complex and ω is the oscillation frequency. Then, a_0 is written as (Robinson & Laurmann 1956, p. 496)

$$a_0(t) = U[(B_0 + B_1)C(k) - B_1]e^{i\omega t}. \quad (3.5)$$

(Note that the presentation of Robinson & Laurmann has been adapted to a more common and modern notation.) In equation (3.5), $C(k)$ is Theodorsen's frequency response function, which depends on the reduced frequency $k = \omega b/U$ via

$$C(k) = \frac{H_1^{(2)}(k)}{H_1^{(2)}(k) + iH_0^{(2)}(k)}, \quad (3.6)$$

where $H_n^{(m)}$ is the Hankel function of the mth kind of order n. Finally, the potential-flow coefficients of lift and pitching moment (positive pitching up) at the mid-chord point are written as

$$C_{L_P} = -\frac{\pi}{U^2}(a_0 + a_1) \quad \text{and} \quad C_{M_{0P}} = \frac{\pi}{4U^2}(a_2 - a_0). \quad (3.7a,b)$$

3.2.2. *Viscous correction*

Following the approach of Brown & Stewartson (1970) in the steady problem (described above), we relax the Kutta condition in the unsteady inviscid pressure distribution (3.1) by introducing a correction Γ_v to the Kutta circulation. This additional circulation will naturally introduce a singularity at the trailing edge. Similar to the steady case, there is no means within potential flow to determine the strength of such a singularity (additional circulation); the essence behind the Kutta condition is to remove such a singularity (condition of least singularity (Crighton 1985)). This additional circulation will have two effects on the unsteady inviscid pressure distribution (3.1): (i) a steady-like effect with two singularities at the leading and trailing edges, similar to the B_s term in (2.2); and (ii) an unsteady effect from the interaction with the wake. The latter has a singularity only at the leading edge. As such, the modified pressure distribution can be written as

$$P(\theta, t) - P_\infty = \rho \left[\frac{1}{2}a_0(t) \tan \frac{\theta}{2} + \sum_{n=1}^{\infty} a_n(t) \sin n\theta + \frac{1}{2}B_v(t) \left(\cot \frac{\theta}{2} + a_{0_v}(t) \tan \frac{\theta}{2} \right) \right],$$
$$(3.8)$$

where the correction B_v is related to the additional circulation as $B_v = U\Gamma_v/(2\pi b)$ and a_{0_v} is the total leading-edge singularity effect from the two contributions of Γ_v,

mentioned above. This term has a non-trivial dynamics (there is a non-trivial transfer function from Γ_v to a_{0_v}). It can be determined from potential-flow considerations: it is the a_0 term in the unsteady inviscid pressure distribution (3.1) over the plate due to a bound circulation Γ_v, ignoring the quasi-steady contribution (i.e. the wake effects only). Therefore, similar to the general a_0 term, it cannot be determined analytically for arbitrary kinematics; there is an analytical expression in the special case of harmonic motion ($a_{0_v} = 2C(k) - 1$ (Brown & Cheng 1981)).

To determine the viscous correction B_v, without resorting to the Kutta condition ($B_v = 0$), we use the unsteady triple-deck theory. Approaching the trailing edge ($\theta \to 0$ or $\tilde{x} \to 1$), the inviscid pressure (with the B_v term) is written as

$$P(\tilde{x} \to 1; t) - P_\infty = \rho \left[\left(\frac{1}{2}a_0(t) + 2\sum_{n=1}^{\infty} na_n(t) + \frac{1}{2}B_v(t)a_{0_v}(t) \right) \sqrt{\frac{1 - \tilde{x}}{2}} + \frac{B_v(t)/2}{\sqrt{\frac{1 - \tilde{x}}{2}}} \right].$$
(3.9)

(Equation (3.9) reduces to (2.2) in the work of Brown & Stewartson (1970) for the steady case ($k = 0$).) In this case, $a_n = 0$ for all $n \geqslant 1$, $a_0 = -2U^2\alpha_s$ and $a_{0_v} = 0$, which yields (2.3) in this work. It also reduces to (2.7) in the work of Brown & Daniels (1975) for their case of a harmonically pitching flat plate about its mid-chord point at very high frequency ($k \gg 1$). In this case, a_0 and a_1 (proportional to $\dot{\alpha}$) are neglected with respect to $a_2 = -b^2\ddot{\alpha}/4$, and $a_n = 0$ for all $n > 2$.

The unsteady inviscid pressure (3.9) has the same form as the steady one (2.3) with

$$\alpha_s(t) \equiv \frac{1}{U^2} \left| \frac{1}{2}a_0(t) + 2\sum_{n=1}^{\infty} na_n(t) + \frac{1}{2}B_v(t)a_{0_v}(t) \right|,$$
(3.10)

$$B_v(t) \equiv B_s = -2\epsilon^3\lambda^{-5/4} \left(\frac{1}{2}a_0(t) + 2\sum_{n=1}^{\infty} na_n(t) + \frac{1}{2}B_v(t)a_{0_v}(t) \right) B_e(\alpha_e).$$
(3.11)

This comparison, along with the fact that the time-derivative term does not enter the triple-deck equations, points to the possibility of directly using the steady solution by Chow & Melnik (1976) of the inner-deck equations for the unsteady case with the equivalence shown above, valid in the range $0 < k \ll O(R^{1/4})$. In the above equivalence, if the term $(1/2)a_0 + 2\sum_{n=1}^{\infty} na_n + (1/2)B_v a_{0_v}$ is negative, then the top of the oscillating thin airfoil will correspond to the top of the steady plate; and if it is positive, then the top of the oscillating thin airfoil should correspond to the bottom of the steady plate. In either case, the equivalent steady angle of attack α_s would be positive. In fact, this correspondence has led to the following interesting behaviour: while there is always a significant lift decrease at the trailing-edge stall angle in the steady case as shown in figure 4, there can be either an increase or a decrease in the unsteady lift when α_s reaches the trailing-edge stall value, as shown by Brown & Cheng (1981). The above equivalence was mistakenly performed in Brown & Cheng (1981) – see equations (2.2), (2.9) and (2.12) in their work.

The application procedure will be as follows. The airfoil kinematics will be used to determine the instantaneous values of $a_n(t)$ via the no-penetration boundary condition (3.3) and (3.5). These coefficients will define the equivalent steady angle of attack α_s according to (3.10), which defines α_e according to (2.4), resulting in B_e via the numerical solution of Chow & Melnik (1976). Finally, B_v will be determined from B_e

and the a_n values according to (3.11), which represents the viscous correction to the Kutta condition and consequently to the lift and moment as

$$C_L = -\frac{\pi}{U^2}[a_0 + a_1 + B_v(1 + a_{0_v})] \quad \text{and} \quad C_{M_0} = \frac{\pi}{4U^2}[a_2 - a_0 + B_v(1 - a_{0_v})]. \quad (3.12a,b)$$

This procedure is iterative at each time step because the input (α_s) depends on the output (B_v): to determine α_s, one needs B_v, which would not be determined until α_s is known. However, our computational results show that the B_v contribution to α_s is quite negligible. As such, it is fair to consider the following equivalence instead of (3.10) and (3.11)

$$\alpha_s(t) \equiv \frac{1}{U^2}\left|\frac{1}{2}a_0(t) + 2\sum_{n=1}^{\infty} na_n(t)\right|, \quad B_v(t) \equiv -2\epsilon^3\lambda^{-5/4}\left(\frac{1}{2}a_0(t) + 2\sum_{n=1}^{\infty} na_n(t)\right)B_e(\alpha_e),$$
$$(3.13a,b)$$

which eliminates the need for iteration at each time step.

It should be noted that this procedure admits arbitrary time variation of the airfoil camber (not necessarily harmonic); only a_0 should be modified accordingly instead of using (3.5). Nevertheless, because there might not be exact closed-form expressions for $a_0(t)$ due to other kinematics (e.g. step input), we recommend using (3.5) to construct a viscous frequency response (describing function (Krylov & Bogoliubov 1943)), assuming a weakly nonlinear system, and then using the Fourier transform to obtain the viscous lift force and pitching moment due to an arbitrarily time-varying camber (as shown in Garrick (1938) and Bisplinghoff *et al.* (1996, pp. 282–283)). This procedure is demonstrated in more detail in the next section.

4. Viscous lift frequency response
4.1. *Set-up of the frequency response (describing function)*

The above approach can be used to construct a viscous extension of Theodorsen's function at a given Reynolds number. For practical use, we opt to show such an extension for a pitching–plunging flat plate. In this case, the normal velocity of the plate (assuming small disturbances $\dot{h}$ and α) is written as

$$v_p(x, t) = \dot{h}(t) - \dot{\alpha}(t)(x - ab) - U\alpha, \quad -b \leqslant x \leqslant b, \quad (4.1)$$

where h is the plunging displacement (positive upwards), α is the pitching angle (angle of attack, positive clockwise) and ab represents the chordwise distance from the mid-chord point to the hinge point, as shown in figure 6. This kinematics results in

$$b_0(t) = 2[\dot{h}(t) + ab\dot{\alpha}(t) - U\alpha] = 2v_{1/2}(t), \quad b_1(t) = -b\dot{\alpha}(t) \quad \text{and} \quad b_n = 0 \quad \forall\, n > 1,$$
$$(4.2a-c)$$

where $v_{1/2}$ is the normal velocity of the mid-chord point. As such, for the harmonic motion

$$h(t) = Hbe^{i\omega t} \quad \text{and} \quad \alpha(t) = A_\alpha e^{i\omega t}, \quad (4.3a,b)$$

equations (3.3) and (3.5) result in the following coefficients:

$$a_0(t) = U[2V_{3/4}C(k)e^{i\omega t} + b\dot{\alpha}(t)], \quad a_1(t) = b\dot{v}_{1/2} - bU\dot{\alpha}(t), \quad a_2(t) = -\frac{b^2\ddot{\alpha}(t)}{4},$$
$$(4.4a-c)$$

where $v_{3/4}(t) = V_{3/4}e^{i\omega t}$ is the normal velocity at the three-quarter-chord point. Also, the coefficient a_{0_v} is given by (Brown & Cheng 1981)

$$a_{0_v} = 2C(k) - 1. \tag{4.5}$$

Note that in this harmonic formulation, equation (4.4) may yield complex values for the coefficients a_n; the actual coefficients, to be used in the series (3.8), are determined by taking the real parts of those in (4.4). In the common classification proposed by Theodorsen (1935), the coefficient a_0 represents the circulatory contribution while the other two coefficients (a_1, a_2) represent the non-circulatory contribution. The lift coefficient is then written as

$$C_L(t) = \underbrace{\underbrace{-\pi\frac{b\dot{v}_{1/2}(t)}{U^2}}_{non\text{-}circulatory} + \underbrace{2\pi\alpha_{3/4}(t)C(k)}_{circulatory}}_{potential\ flow\ solution} - \underbrace{2\pi\tilde{B}_v(t)C(k)}_{viscous\ correction}, \tag{4.6}$$

where $\tilde{B}_v = B_v/U^2$, $\alpha_{3/4}$ is the local angle of attack at the three-quarter-chord point (as recommended by the Pistolesi theorem (Schlichting & Truckenbrodt 1979, p. 80)), and the multiplication $\alpha_{3/4}(t)C(k)$ is interpreted after writing $\alpha_{3/4}(t) = \overline{\alpha_{3/4}}e^{i\omega t}$ as

$$(\alpha_{3/4}C(k))(t) = \text{Re}(\overline{\alpha_{3/4}}C(k)e^{i\omega t}), \tag{4.7}$$

where $\overline{\alpha_{3/4}}$ may be a complex number and $\text{Re}(\cdot)$ denotes the real part of its complex argument.

Recall that if $u(t) = Ae^{i\omega t}$ is the input to a linear dynamical system whose frequency response is $G(i\omega)$, then the steady-state output is simply written as $y(t) = A|G(i\omega)|e^{i\omega t + \arg G(i\omega)}$ (Ogata & Yang 1970). The describing function technique represents an extension of the frequency response concept for weakly nonlinear systems (Krylov & Bogoliubov 1943). In this technique, only the response at the fundamental frequency is considered and the higher harmonics are neglected. As such, the response of a weakly nonlinear system to the input $u(t) = Ae^{i\omega t}$ is approximated as $y(t) = Y(A, \omega)e^{i\omega t + \phi(A,\omega)}$. That is, unlike linear systems, the magnitude and phase of the transfer function depend on the input amplitude. Using such a technique, we provide below a viscous extension of Theodorsen's frequency response, i.e. the frequency response between the quasi-steady lift (input) and the viscous circulatory lift (output).

The system possesses two nonlinearities as shown in figure 8: a multiplicative nonlinearity and the triple-deck viscous nonlinearity. The former is due to interactions between the airfoil motion (represented by the a_n) and the trailing-edge singular behaviour (represented by B_s) while the latter is due to the steady triple-deck nonlinear characteristics, determined numerically by Chow & Melnik (1976), and shown here in figure 3(b). The effect of these nonlinearities is minimal with respect to the main linear contribution at small angles of attack as evident from the power spectra (fast Fourier transform, FFT) of the total circulatory lift coefficient C_{L_C} shown in figure 7(a) for the case of pitching around the mid-chord point with $A_\alpha = 1°$ at $k = 0.8$ and $R = 10^5$. The FFT of C_{L_C} has a single distinct peak at the operating frequency ($k = 0.8$). In fact, even the viscous contribution (the B_v term) is mostly linear despite the existence of a weak cubic nonlinearity as evident from its FFT
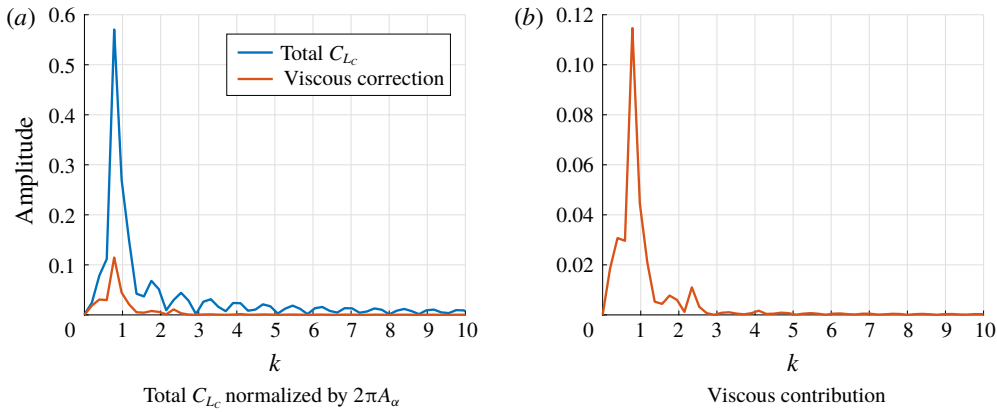
FIGURE 7. (Colour online) Power spectra (FFT) of (*a*) the total circulatory lift coefficient C_{Lc} and (*b*) the viscous correction $2\pi\tilde{B}_v C(k)$, both normalized by $2\pi A_\alpha$, for the case of a flat plate pitching around the mid-chord point with $A_\alpha = 1°$ at $k = 0.8$ and $R = 10^5$. The behaviour is almost linear with a single distinct peak at this small amplitude.
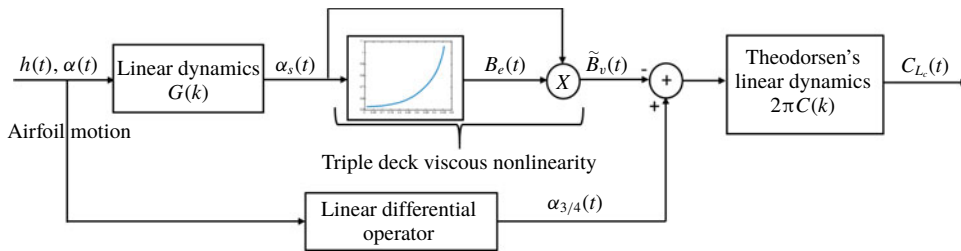

FIGURE 8. (Colour online) A block diagram showing the different components constituting the dynamics of the viscous circulatory lift. The airfoil motion dictates the angle of attack $\alpha_{3/4}$ at the three-quarter-chord point, which is the main input to Theodorsen's inviscid linear dynamics, resulting in the potential-flow circulatory lift. The upper branch represents the viscous correction developed in this work. The correction term $\tilde{B}_v$ represents a singularity in the inviscid pressure distribution at the trailing edge. It should be set to zero according to the Kutta condition. Rather, it is obtained here from the triple-deck boundary layer theory. The airfoil motion goes into some linear dynamics (that includes the Theodorsen function) to obtain an equivalent steady angle of attack, which will be used in the nonlinear triple-deck theory to obtain the viscous correction to the circulatory lift.

shown in figure 7(*b*). This weakly nonlinear behaviour of the system justifies the use of the describing function approach (akin to linearization) to construct a frequency response. It is interesting to note that the triple-deck theory confirms the common expectation that the most significant term in the power series expansion of lift in terms of the angle of attack after the linear term is the cubic one (Librescu, Chiocchia & Marzocca 2003; Ding & Wang 2006). It is also interesting to point out that even at this small amplitude ($A_\alpha = 1°$) and relatively large Reynolds number ($R = 10^5$), the viscous contribution is approximately 19 %, as shown in figure 7(*a*).

4.2. *Computation procedure*

Let k and R be given. Then, the quasi-steady lift coefficient (input to the sought lift dynamical system) is written as

$$C_{L_{QS}}(t) = 2\pi\alpha_{3/4}(t). \tag{4.8}$$

Also, the coefficients a_0, a_1 and a_2 are given from (4.4). Thus, α_s can be obtained accordingly from (3.13); however, care should be taken when applying (3.13). It should be applied instantaneously as

$$\alpha_s(t) = \frac{1}{U^2} \left| \frac{1}{2}a_0(t) + 2a_1(t) + 4a_2(t) \right|. \tag{4.9}$$

The scaled angle of attack $\alpha_e(t)$ for the numerical solution of Chow & Melnik (1976) is obtained from (2.4) with $\epsilon = R^{-1/8}$. Using figure 3(*b*), one can obtain $B_e(t)$, which in turn is substituted in (3.13) to determine the viscous correction $B_v(t)$. The unsteady viscous circulatory lift coefficient is determined from (4.6) by excluding the first term, i.e.

$$C_{L_C}(t) = 2\pi \operatorname{Re}[(\alpha_{3/4}(t) - \tilde{B}_v(t))C(k)]. \tag{4.10}$$

Finally, a spectral analysis (e.g. FFT) is applied to $C_{L_C}(t)$ to extract its relative amplitude and phase shift with respect to $C_{L_{QS}}(t)$. That is, the circulatory lift viscous transfer function C_v is defined as

$$C_v(k; R) \triangleq \frac{C_{L_C}(k; R)}{C_{L_{QS}}(k)}. \tag{4.11}$$

Figure 8 shows a block diagram for the dynamics of the unsteady viscous circulatory lift.

Note that if $\alpha_e(t)$ exceeds 0.47, then the simulation should be terminated because such a value implies trailing-edge stall beyond which the current analysis is not valid. This limitation defines the region of applicability of the developed model. For example, the model can handle an oscillation about the mid-chord point with $3°$ amplitude at 0.4 reduced frequency and 10 000 Reynolds number. However, it cannot handle the same situation when the amplitude is increased to $4°$ as $\alpha_e(t)$ would exceed 0.47 during the course of the simulation.

Following the above procedure, we construct frequency responses of the unsteady, viscous, circulatory lift coefficient C_{L_C} at different Reynolds numbers, which are shown in figure 9 in comparison to Theodorsen's. Intuitively, as R increases, the viscous response approaches the inviscid Theodorsen's response and *vice versa*. The viscous lift transfer function has a smaller magnitude than the inviscid Theodorsen's solution as R decreases. Moreover, it is found that viscosity induces a significant phase lag beyond Theodorsen's; the larger the oscillation frequency and the smaller the Reynolds number, the larger is the discrepancy between Theodorsen's phase lag and the viscous results. Interestingly, this finding supports the conclusions of some of the earlier experimental efforts (Chu & Abramson 1959; Bass *et al.* 1982): Chu & Abramson (1959) suggested adding a phase lag of $-10°$ to the Theodorsen function for a better estimate of the unsteady lift and flutter boundary when $k \simeq 0.5$. Bass *et al.* (1982) conducted a water tunnel experiment for a NACA 16-012 undergoing pitching oscillations around its quarter-chord point in the range of $0.5 < k < 10$ and $R = 6500$–$26\,500$. They compared their force measurements to Theodorsen's
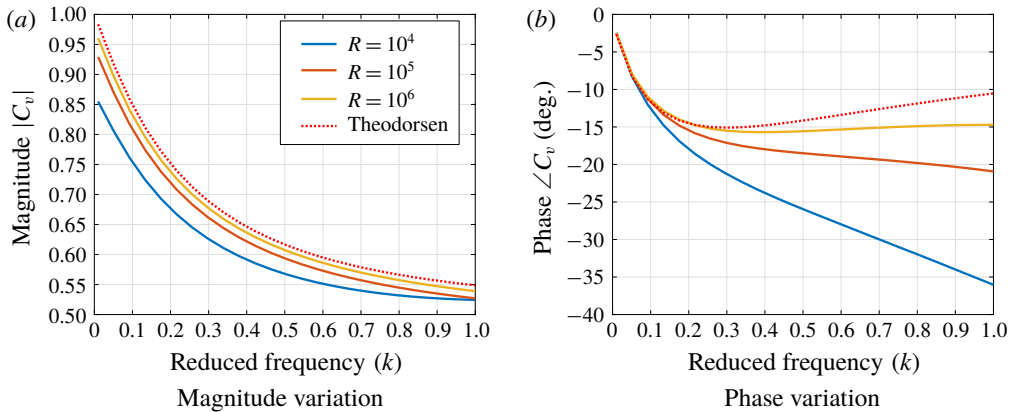
FIGURE 9. (Colour online) Comparison between the frequency responses of the unsteady, viscous, circulatory lift coefficient C_{L_C} at different Reynolds numbers and that of the potential-flow circulatory lift coefficient (i.e. Theodorsen's): (*a*) magnitude variation; (*b*) phase variation. The larger the frequency and the lower the Reynolds number, the larger is the discrepancy in phase between Theodorsen's function and the viscous frequency response.

potential-flow frequency response. They found bad agreement in the range $0.5 < k < 2$ where the most pronounced boundary layer activity is observed and the flow near the trailing edge being separated and alternating around the trailing edge. They concluded that adding a phase lag of $-30°$ to the Theodorsen's $C(k)$ would make the predicted lift from the classical theory of unsteady aerodynamics match their experimental measurements over this range, which supports the current results shown in figure 9.

This finding is particularly important for the determination of the flutter boundary (e.g. Alben 2008; Mandre & Mahadevan 2010; Zakaria, Al-Haik & Hajj 2015; Hussein & Canfield 2017). Note that the flutter instability, similar to any typical Hopf bifurcation, is mainly dictated by when energy is added/subtracted during the cycle. That is, the phase difference between the applied loads (aerodynamic loads) and the system motion (e.g. angle of attack) plays a crucial role in dictating the stability boundary (Bisplinghoff *et al.* 1996, p. 280). Therefore, if the Theodorsen function does not capture such a phase difference correctly, it will typically lead to an erroneous flutter stability boundary. Hence, if the current model better captures the phase lag, it may enhance our flutter predictability, if occurring at high reduced frequencies. Based on this discussion, we suggest using the obtained viscous frequency responses in place of Theodorsen's for a more accurate, yet efficient, estimate of the flutter boundary. This point will be discussed further below from an added-mass point of view in the last section.

5. Validation via computational simulation

In this section, we investigate the effect of viscosity on the lift frequency response using a higher-fidelity simulation of the Navier–Stokes equations to support or refute the theoretical findings in the last section. Although the developed theory should be valid only for the laminar regime, it is interesting to assess its performance in high-Reynolds-number turbulent flows as well to investigate its ability to capture the global picture of the flow field and some important integrated quantities such as

the generated aerodynamic loads. For this purpose, two computational set-ups have been constructed using the finite-volume-based software package ANSYS Fluent: (1) unsteady laminar simulation and (2) unsteady Reynolds-averaged Navier–Stokes (URANS). For the latter set-up, it is important to select an appropriate turbulence model that accurately captures the behaviour of the integrated global quantities of interest (e.g. the lift dynamics). Note that details of the small-scale features in the flow will not be captured by averaging; large-eddy or direct numerical simulations will be needed instead. However, this is beyond the scope of this paper. The k–ω turbulence model is well known for its superiority in handling complex boundary layer flows with adverse pressure gradients (Menter 1994; Wilcox 1998). However, it may result in early transition and separation and is sensitive to inlet boundary conditions. Nevertheless, no severe adverse pressure gradient and separation are expected in the current investigations with small amplitudes. We also assume a fully turbulent flow in the high-Reynolds-number simulation cases (i.e. no transition). Therefore, the k–ω model should be quite suitable for the current application, with the caveat of being sensitive to free-stream inlet conditions. This issue is resolved by selecting its extension, the shear stress transport (SST) k–ω model, which makes use of the k–ω model near the wall and the k–ϵ model in the free stream and wake regions. As such, the k–ω SST exploits the k–ω capabilities in capturing the boundary layer and its adverse pressure gradient while mitigating its sensitivity to inlet conditions (such as the free-stream turbulence intensity). Hence, it is an almost perfect choice for the current study when performing simulations at high Reynolds numbers, assuming a fully turbulent flow.

In relation to the numerical set-up, the pressure–velocity coupling was considered by the SIMPLE algorithm. All the spatial discretizations were second-order upwind. Implicit second-order discretization was chosen for transient terms. The convergence criteria for all the variables were set to be 10^{-6} at each time step. To select an appropriate value for the time step, three numerical simulations were performed using 500 points, 250 points and 150 points per cycle. It was found that 250 samples per cycle is sufficient to obtain well-converged results. In each simulation, the number of cycles is chosen to be sufficient for a periodic lift pattern to establish.

5.1. *Computational set-up*

The O-type far field located $25c$ away from the solid body has been implemented for grid generation around the standard NACA 0012 airfoil with sharp trailing edge. In return of closing the blunt trailing edge of the original NACA 0012, the thickness of the airfoil altered to 11.9 %. To construct the dynamic mesh due to the airfoil motion, the computational domain is divided into three rings as shown in figure 10. The inner ring (red), which encloses the airfoil, has the radius of $6c$. In this region, a hybrid mesh is used such that a boundary layer structure dense mesh near the airfoil guarantees $y+ < 1$, in conjunction with an unstructured tri-mesh attached to it. The distance of the first layer of the mesh was set to be $10^{-5}c$ with 1.1 growth factor, which guarantees that the triple-deck structure, $O(R^{-3/4})$, is well resolved at the highest Reynolds number (10^6) in this simulation. A total of 300 mesh points were used on each side of the airfoil. A size function has been used to ensure that the unstructured mesh in the inner ring is dense enough to capture the shed vortices if needed. The whole inner ring including the airfoil undergos a rigid-body pitching motion. No dynamic mesh is used in this region to ensure that the grids near the airfoil maintain their fine configuration and quality as they were before the motion.
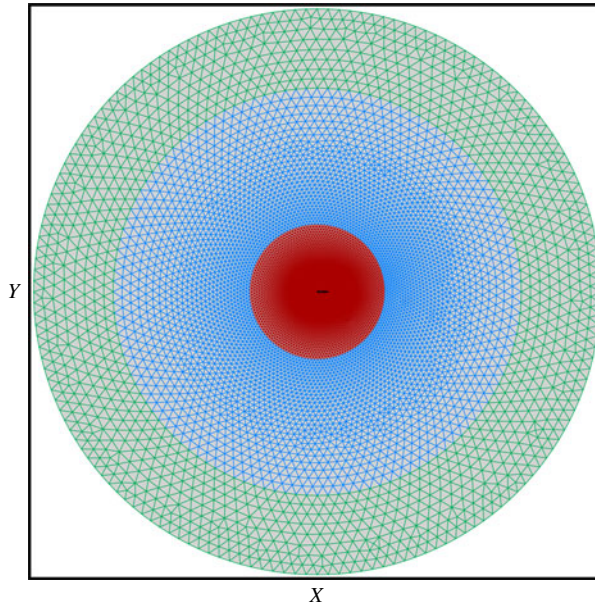
FIGURE 10. (Colour online) O-type mesh around the airfoil: the outer ring is fixed, the inner ring moves rigidly with the airfoil, and the intermediate ring represents the deforming dynamic mesh.

The outer ring located at $25c$ away from the airfoil is stationary as if no motion is taking place inside the domain. This fixed mesh near the outer boundaries certifies that the far-field boundary conditions are applied correctly. The intermediate ring plays the main role of the dynamic mesh. The inner radius of this ring is $6c$ and the outer radius is $18c$; it occupies a large region inside the domain. Both remeshing and deforming techniques are utilized to damp the deformations in the region caused by the motion of the inner ring. A user-defined function is attached to the solver to impose an arbitrary motion to the airfoil and prevent high skewness in the dynamic mesh zone. The advantage of this method may not be sensible when deflections are small, yet it demonstrates its ability in damping mesh deformations at large motion amplitude. The large size of the intermediate region gives enough room to handle excessive deflections. It has to be pointed out that the position of each ring has been chosen based on numerous simulations. The total number of grids is roughly 2×10^5. For more information about the computational set-up, the reader is referred to our earlier effort (Rezaei & Taha 2017). A mesh independence study has been performed by running another case in which the grids were twice as dense, and no alteration in the results has been observed. Thus, the aforementioned mesh configuration was utilized in all of the forthcoming simulations.

Since the flow is assumed to be incompressible, the velocity inlet and pressure outlet, corresponding to the left semicircle and right semicircle, respectively, were set as the far-field boundary conditions. The chord length of the airfoil is 18 cm and the magnitude of the velocity at the inlet boundary is 10 m s^{-1} and 1 m s^{-1}, corresponding to $R = 10^5$ and $R = 10^4$, respectively. The turbulent intensity of the flow was set to 0.1 % and the gauge pressure at the outlet boundary condition was set to zero. Note that the free-stream turbulence intensity is not expected to significantly
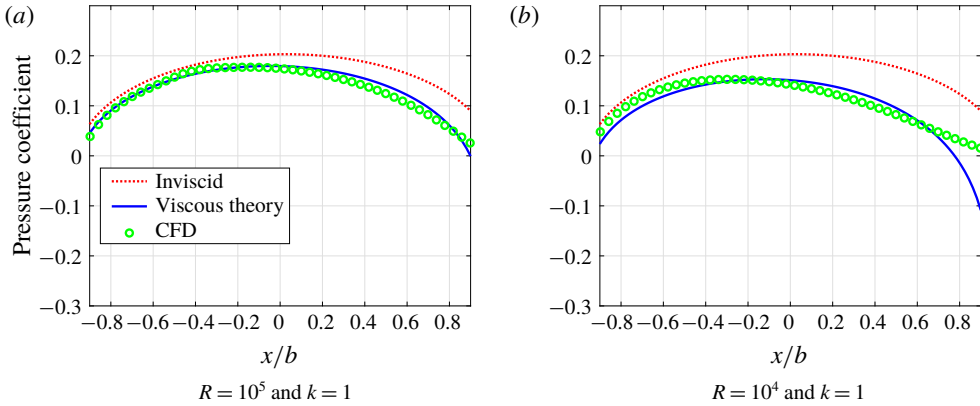
FIGURE 11. (Colour online) Comparison of the pressure distribution over the flat plate from the inviscid theory, the current viscous theory and computational simulations in the case of a harmonically pitching airfoil about its quarter-chord with $3°$ amplitude at $k = 1$ and (*a*) $R = 10^5$ and (*b*) $R = 10^4$. In the former case, a URANS solver is used whereas a laminar solver is used in the latter case. The panels show the pressure distributions at the instant of zero pitching angle $\alpha(t) = 0$ and maximum upward pitching velocity $\dot{\alpha}$.

affect the results because the k–ω SST turbulence model utilizes the k–ϵ model in the free-stream region, which is robust to changes in the inlet conditions. Our simulations with changing the inlet turbulence intensity 10-fold did not show an appreciable change in the lift dynamics. The no-slip boundary condition is imposed on the airfoil which is undergoing the harmonic pitching motion $\alpha = A_\alpha \sin \omega t$ with a pitching amplitude of $A_\alpha = 3°$ to ensure that the airfoil is in the pre-stall regime (Schlichting & Truckenbrodt 1979).

Figure 11 shows the distribution of the pressure difference (i.e. lift distribution) over the flat plate for the case of pitching about the quarter-chord with $3°$ amplitude at $k = 1$ for two Reynolds numbers, $R = 10^5$ and $R = 10^4$. Figure 11 shows results from the inviscid theory (i.e. twice the result of (3.1)), which is insensitive with respect to R; the developed viscous theory (i.e. twice the result of (3.8)); and the computational simulations described above. URANS is used in the case of the relatively high $R = 10^5$ and the laminar solver is used at the lower Reynolds number $R = 10^4$. Very good matching between the computational simulations and the developed theory is found. It should be noted that the selected instant ($\alpha(t) = 0$ and $\dot{\alpha}$ maximum) is a critical instant during the cycle where the flat plate is on the verge of trailing-edge stall, as shown in figure 12: when $\alpha(t) = 0$ and $\dot{\alpha}$ is maximum, at this relatively high k, the equivalent α_e becomes very close to the trailing-edge stall value 0.47. Both results from computational simulations and the current boundary layer theory indicate that, as R decreases, the pressure distribution at this critical moment deviates more from the inviscid one; the pressure distribution decreases and shifts to the left (i.e. the pressure attains its maximum earlier on the airfoil). The developed theory captures this behaviour by adding a singularity at the trailing edge, which bends the pressure distribution curve downwards and to the left. However, it is precisely this trailing-edge singularity that causes the discrepancy between the predicted singular pressure and the actual non-singular pressure at the trailing edge. Nevertheless, the strength of this singularity decreases as R increases and the discrepancy becomes more confined to the immediate vicinity of the trailing edge (i.e. agreement with
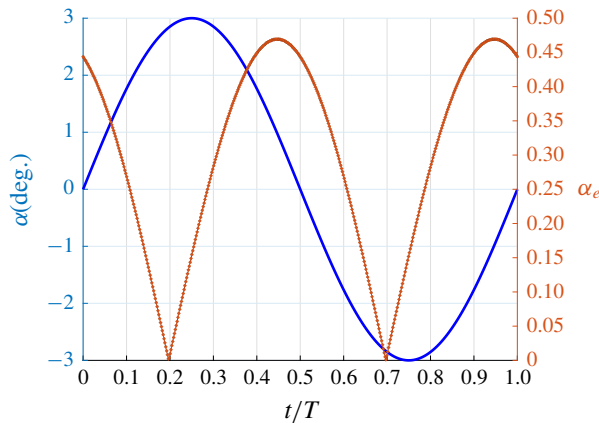
FIGURE 12. (Colour online) Variation of the equivalent angle of attack α_e over the cycle along with the actual angle of attack α for the case of a harmonically pitching flat plate about its quarter-chord with $3°$ amplitude at $k = 1$ and $R = 10^4$. At this relatively high k, the instant of maximum $\dot{\alpha}$ renders the airfoil on the verge of trailing-edge stall in comparison to the instant of the maximum α.

the computational simulations over a wider range of the airfoil). We emphasize that the developed theory should be valid only for high Reynolds numbers. In other words, the results of the developed theory should be interpreted only as providing a first-order correction to the inviscid results for finite Reynolds numbers; from this point of view, it is quite satisfactory. One more point that is noteworthy, though it does not seem to be significant here, is that the developed theory is for an infinitely thin airfoil whereas the computational simulations are performed for a finite-thickness airfoil (NACA 0012).

5.2. *Computation of the viscous lift frequency response function*

In this study, we show how the viscous lift frequency response (describing function) is determined from computational simulations at a given Reynolds number. Similar to Theodorsen (1935), this transfer function is defined as the ratio between the circulatory lift coefficient and the quasi-steady lift coefficient. As such, given a combination of k and R, our computational set-up is simulated to result in a time history of the total lift coefficient $C_{L_{tot}}$. According to the describing function approach (Krylov & Bogoliubov 1943), the Fourier transform $\hat{C}_{L_{tot}}$ of the total lift coefficient at the fundamental frequency k is considered; it is a complex number, as shown in figure 13. To extract the circulatory contribution $\hat{C}_{Lc}$ from $\hat{C}_{L_{tot}}$, the non-circulatory contribution must be subtracted. Adopting Theodorsen's estimate for the non-circulatory loads in the case of a pitching airfoil around the quarter-chord point, we obtain

$$C_{L_{NC}} = \pi \frac{b}{U} \left(\dot{\alpha} + \frac{b\ddot{\alpha}}{2U} \right) \quad \Longrightarrow \quad \hat{C}_{L_{NC}}(k) = \pi A_\alpha (ik - k^2/2). \quad (5.1)$$

(Theodorsen's estimate for the non-circulatory loads may not be accurate, as will be discussed below.) As such, the circulatory lift frequency response is obtained as $\hat{C}_{Lc} = \hat{C}_{L_{tot}} - \hat{C}_{L_{NC}}$, as shown graphically in figure 13. Then, the complex number $\hat{C}_{Lc}$ is
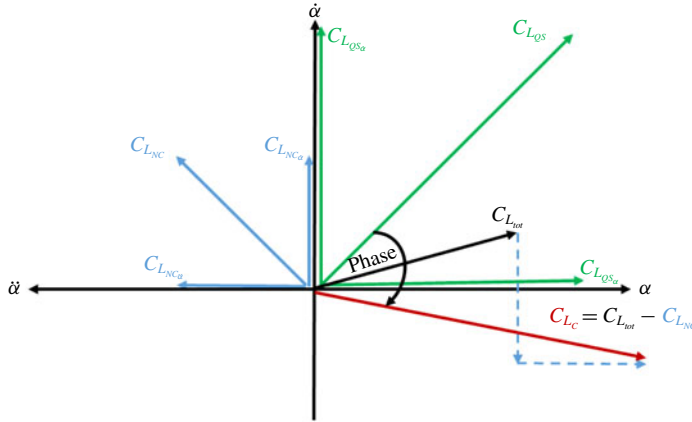
FIGURE 13. (Colour online) Complex plane showing the different lift components.

divided by the quasi-steady lift

$$C_{L_{QS}} = 2\pi\alpha_{3/4} = 2\pi\left(\alpha + \frac{\dot{\alpha}b}{U}\right) \implies \hat{C}_{L_{QS}} = 2\pi A_\alpha\left(1 + ik\right) \qquad (5.2)$$

to obtain the viscous lift transfer function $C_v(k; R) = \hat{C}_{L_C}(k; R)/\hat{C}_{L_{QS}}(k)$.

Figure 14 shows the computed viscous lift frequency response function at two different Reynolds numbers, $R = 10^5$ and $R = 10^4$; the former is obtained using URANS and the latter is obtained using the laminar solver. Figure 14 also shows the inviscid Theodorsen's lift frequency response function and the developed viscous extension for comparison. For the case of $R = 10^4$, the convergence properties of the laminar solver at lower k values were not satisfactory and are therefore omitted. It is found that the magnitude of the transfer function decreases, as R decreases and k increases, more than what is predicted by the triple-deck theory (conforming with the results of Zakaria, Taha & Hajj (2017)). However, the computational phase results corroborate the theoretical findings discussed above. That is, at lower Reynolds numbers and higher frequencies, there is a significant deviation from Theodorsen's phase prediction. In fact, there is a satisfactory quantitative agreement between the theoretical phase lag predictions and computational results. This additional phase lag may significantly affect the prediction of an instability boundary (e.g. flutter) as discussed above. Note that Bisplinghoff *et al.* (1996, p. 280) emphasized the importance of unsteady phase lag in dictating the flutter boundary even at low reduced frequencies (e.g. $k = 0.1$) where the phase lag is already very small. Therefore, since the developed theory provides a better estimate of the unsteady phase lag than the Theodorsen function, particularly at large k and low R, it is expected to enhance our retarding capability in predicting flutter, which is discussed further below from an added-mass point of view. It should be noted that most of the earlier experimental efforts that reported failure in predicting flutter (or unsteady loads) lie in the high-frequency range: $k \simeq 0.5$ (Chu & Abramson 1959), $k \simeq 0.6$–1.4 (Henry 1961), $k \simeq 0.7$ (Abramson & Ransleben 1965) and $k \simeq 0.5$–10.0 (Bass *et al.* 1982). Therefore, it is expected that the developed theory may help to reconcile the concerns raised in these efforts; a quantitative assessment of the effect of the predicted additional phase lag on the flutter boundary will be addressed in future work. Having said that, one
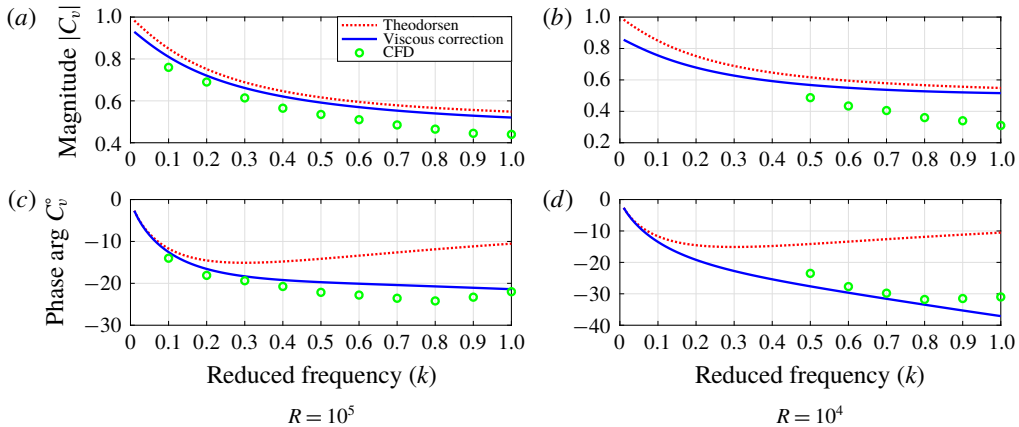
FIGURE 14. (Colour online) Computational results of the frequency responses of the unsteady, viscous, circulatory lift coefficient C_{L_C} at different Reynolds numbers. The computational results support the theoretical finding that the larger the frequency and the lower the Reynolds number, the larger is the discrepancy in phase between Theodorsen function and the viscous frequency response.

should emphasize that the flutter frequency of conventional airplane wings is usually of the order of $k = 0.1$ (Bisplinghoff *et al.* 1996, p. 280), for which the current theory results in a phase close to Theodorsen's. However, it is expected that the developed theory will be useful for the flutter prediction of the next-generation unconventional designs with highly flexible wings (typically with higher flutter frequencies).

It is noteworthy to mention that a better matching between the theoretical phase lag predictions and computational results is obtained when using the eddy viscosity in the developed boundary layer theory, as shown in figure 15 for the case of $R = 10^6$. In this case, a Reynolds number based on the average value of the eddy viscosity (obtained from the URANS simulations over a domain close enough and surrounding the airfoil) is used in the developed theoretical model. That is, even when operating at a high Reynolds number where the deviations between Theodorsen results and the developed theory and computational simulations are minimal, the effective Reynolds number is actually less, implying that the phase predictions of the Theodorsen function are quite off at high frequencies. Note that, as R decreases, the turbulent viscosity ratio decreases and its effect on the developed theory may be neglected.

6. Physical illustrations: viscosity-induced lag and the Kutta condition

6.1. *Viscosity-induced lag*

The fact that viscosity induces phase lag in the flow response is well known from classical fluid problems. For example, the laminar viscous flow in a pipe due to an oscillatory pressure gradient shows a phase lag between the input pressure gradient and the flow response (e.g. velocity distribution, wall shear or vorticity (Langlois & Deville 2014, pp. 113–116)). Also, recall the Stokes second problem: the flow above an oscillating infinite plate, shown in figure 16. This problem is one of the few simple problems where an analytical solution of the Navier–Stokes equations is available (Lamb 1932, pp. 619–623; Batchelor 2000, pp. 191–193; Langlois & Deville 2014, pp. 109–111), which results in the following velocity distribution:

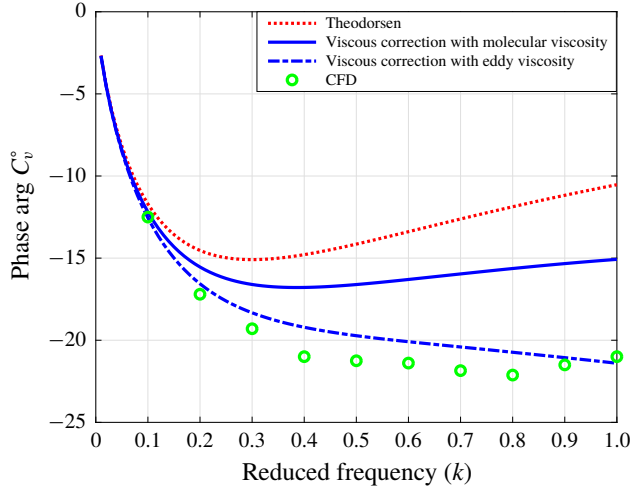$$u(y, t) = U e^{-y/\delta} \cos(\omega t - y/\delta), \tag{6.1}$$

FIGURE 15. (Colour online) Phase of the lift frequency response at $R = 10^6$ when using molecular and eddy viscosity. Using eddy viscosity enhances the matching between the theoretical phase lag predictions and computational simulations. A turbulent viscosity ratio of 10 is used based on URANS simulations.
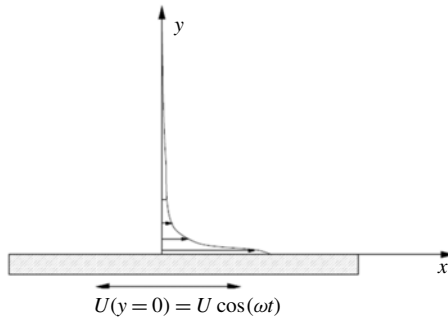

FIGURE 16. Stokes second problem: flow above an oscillating infinite plate.

where $\delta = \sqrt{2\nu/\omega}$ is the thickness of the boundary layer (Stokes layer) and ν is the fluid's kinematic viscosity. Equation (6.1) clearly shows the phase lag between the input (plate motion) to the flow dynamics and the flow response and that this phase lag increases with the fluid viscosity. Moreover, the vorticity in the boundary layer experiences even more lag in development with respect to the plate motion than the fluid velocity as shown in the vorticity response:

$$\zeta(y, t) = -\frac{\partial u}{\partial y} = \frac{\sqrt{2}U}{\delta} e^{-y/\delta} \cos(\omega t - y/\delta - \pi/4). \tag{6.2}$$

The generation of vorticity in the boundary layer is particularly important for the explanation of the observed lag in the lift frequency response of an oscillating airfoil, for the lift evolution is intimately related to vorticity generation and circulation development.
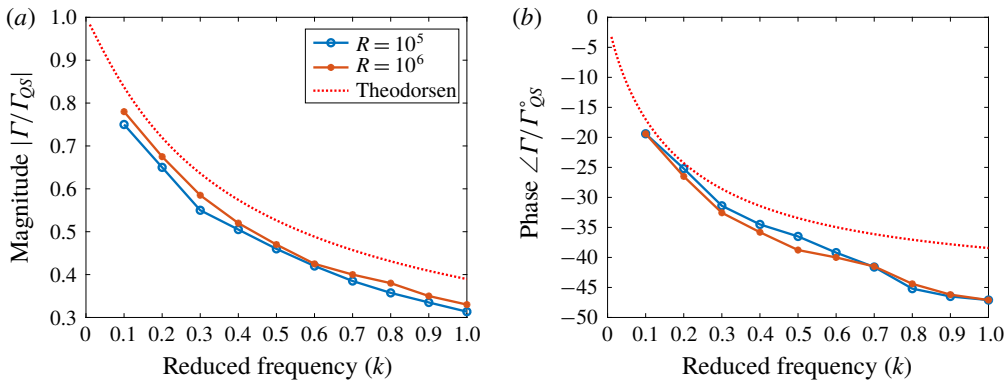
FIGURE 17. (Colour online) Computational results of the frequency responses of the unsteady, viscous, bound circulation at different Reynolds numbers: (*a*) magnitude variation and (*b*) phase variation. A behaviour similar to the circulatory lift frequency response is observed: the larger the frequency, the larger is the discrepancy in phase between inviscid and viscous responses.

6.2. *Viscous damping and lag in circulation development*

To show that the observed phase lag in the lift frequency response is due to lag in the development of the bound circulation, we computed the latter by performing a line integral of the tangential velocity along a closed contour around the airfoil. Then, we followed a similar procedure to the one presented in the last section to construct a frequency response (describing function) between the quasi-steady circulation Γ_{QS} as an input and the viscous unsteady bound circulation Γ as an output. The former is determined as

$$\Gamma_{QS} = UbC_{L_{QS}} = 2\pi bU\left(\alpha + \frac{\dot{\alpha}b}{U}\right) \quad \implies \quad \hat{\Gamma}_{QS} = 2\pi UbA_\alpha(1 + \mathrm{i}k). \qquad (6.3)$$

Figure 17 shows a comparison between the viscous transfer function $\hat{\Gamma}/\hat{\Gamma}_{QS}$ of the circulation response from computational simulations and the corresponding potential-flow one, which is different from the Theodorsen function $C(k)$. Rather, it is given as (Bisplinghoff *et al.* 1996, pp. 275–276)

$$\frac{\hat{\Gamma}_P}{\hat{\Gamma}_{QS}}(k) = \frac{-2\mathrm{e}^{-\mathrm{i}k}}{\mathrm{i}k\pi(\mathrm{H}_1^{(2)}(k) + \mathrm{i}\mathrm{H}_0^{(2)}(k))}, \qquad (6.4)$$

where Γ_P denotes the potential-flow unsteady bound circulation. Similar to the lift transfer function $C_v(k; R) = \hat{C}_{L_C}(k; R)/\hat{C}_{L_{QS}}(k)$, the circulation transfer function $\hat{\Gamma}/\hat{\Gamma}_{QS}$ experiences more phase lag due to viscosity at high frequencies than its potential-flow counterpart.

Figure 18 shows the vorticity contours during the cycle of a harmonically pitching NACA 0012 airfoil about its quarter-chord with $3°$ amplitude at $k = 1$ and two different Reynolds numbers, $R = 10^5$ and $R = 10^4$. First, figure 18(*a*) shows that for this relatively high k, the wake is more deformed at the instants of zero pitching angle ($\alpha = 0$) and maximum angular velocity $\dot{\alpha}$ in comparison to the instants of maximum α with $\dot{\alpha} = 0$. This fact, similar to the theoretical findings above, implies
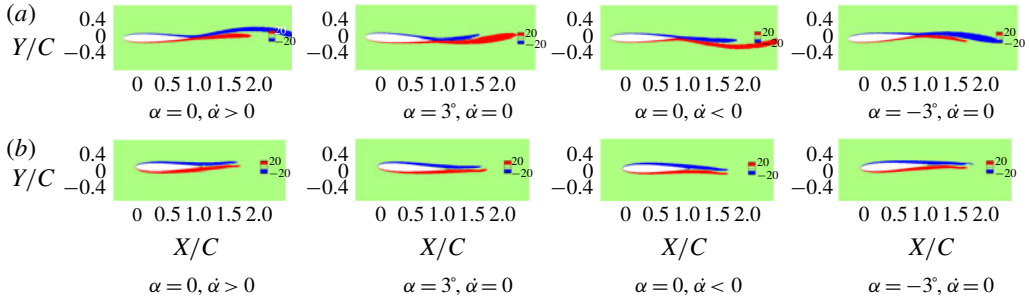
FIGURE 18. (Colour online) Vorticity contours $(1 \ \text{s}^{-1})$ during the cycle of a harmonically pitching NACA 0012 airfoil about its quarter-chord with $3°$ amplitude at $k = 1$ and (*a*) $R = 10^5$ and (*b*) $R = 10^4$. As R decreases, viscosity damps the deformation of wake vorticity.
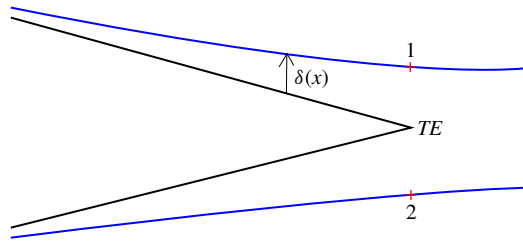

FIGURE 19. (Colour online) A zoom at the trailing edge and its boundary layer. The blue lines represent the edge of the boundary layers and the red dots (points 1 and 2) represent the edge of the boundary layers at the trailing-edge x station. The potential-flow theory, ignoring the boundary layers, assumes that points 1 and 2 and the trailing edge all lie on top of each other. Hence, the Kutta condition (continuous pressure at the trailing edge) would dictate $P_1 = P_2$ neglecting the pressure rise across the boundary layer and its effect on the circulation development over the airfoil.

that the airfoil would be more prone to trailing-edge stall at the instants of maximum $\dot{\alpha}$ when oscillating at high frequencies. Second, the comparison between the two sets of figures at the two values of R indicates a much smaller wake activity (deformation) for lower R, which is intuitively expected due to viscous damping. From a dynamical system perspective, this damping of wake vorticity will be typically associated with lag in its development which, via conservation of circulation, points to a lag in the bound circulation development. Therefore, it may explain the larger phase lag of the lift frequency response found at lower Reynolds numbers and higher frequencies.

6.3. *Lag in circulation development and the Kutta condition*

One may be able to relate the observed lag in the circulatory lift frequency response (due to lag in the circulation development) to the Kutta condition. Note that the trailing-edge singularity term in the pressure distribution (3.8) is the main modification introduced to the inviscid pressure distribution (3.1). Therefore, the observed additional lag in the lift response may be related to the pressure near the trailing edge, which motivates the following analysis.

The Kutta condition at the sharp trailing edge can be stated in several ways, such as (i) finite velocity, (ii) zero loading or (iii) continuous pressure, among others (see

Sears 1956). In fact, some of these representations are, indeed, exact. For example, clearly, the pressure must be continuous at the trailing edge (TE). That is,

$$\lim_{y \to 0^+} P(TE, y) = \lim_{y \to 0^-} P(TE, y). \tag{6.5}$$

However, the inviscid pressure distribution over the plate represents the distribution at the edge of the boundary layer. That is, applying the condition (6.5) within the framework of potential-flow results in $P_1 = P_2$, where the points 1 and 2 lie on the edge of the boundary layer at the trailing-edge station as shown in figure 19. While Prandtl's boundary layer assumption (pressure is constant along the boundary layer thickness) is valid over the majority of the airfoil length, it is not necessarily valid in the singular trailing-edge region. As such, if ΔP is the pressure rise across the boundary layer, then the condition (6.5) results in

$$P_1 - \Delta P_1 = P_2 - \Delta P_2, \tag{6.6}$$

which is also suggested by Preston (1943) and Spence (1954) as a modification of the classical Kutta condition ($P_1 = P_2$). Since the points 1 and 2 lie on the edge of the boundary layer, one can use the unsteady Bernoulli's equation to relate P_1 and P_2 as (Bisplinghoff *et al.* 1996; Katz & Plotkin 2001)

$$\frac{P_1}{\rho} + \frac{1}{2}V_1^2 + \frac{\partial \phi_1}{\partial t} = \frac{P_2}{\rho} + \frac{1}{2}V_2^2 + \frac{\partial \phi_2}{\partial t}, \tag{6.7}$$

where V is the potential-flow velocity at the edge of the boundary layer and ϕ is the corresponding velocity potential. Combining (6.6) and (6.7) and realizing that $\phi_1 - \phi_2 = \Gamma$, one obtains

$$\dot{\Gamma} = \frac{1}{2}(V_2^2 - V_1^2) + \frac{\Delta P_2 - \Delta P_1}{\rho}. \tag{6.8}$$

Equation (6.8) represents an exact (derived) version of the hypothesized Kutta condition. In particular, it governs the evolution of the bound circulation over the airfoil, i.e. it provides the dynamics of the bound circulation. Interestingly, it can be derived from a completely different point of view than the continuity argument (6.5) which we opt to show below. The underpinning concept is that the circulation is instantaneously conserved. That is, the instantaneous rate of change of circulation $\dot{\Gamma}$ is related to the total vorticity flux at separation (Sears 1976). As such, assuming that separation occurs at the trailing edge (complying with the triple-deck theory used in this paper), we write

$$\dot{\Gamma} = -\left[\int_0^{\delta_1} \zeta(y)u(y)\,\mathrm{d}y + \int_{-\delta_2}^0 \zeta(y)u(y)\,\mathrm{d}y \right], \tag{6.9}$$

where ζ is the clockwise vorticity, u is the velocity parallel to the wall inside the boundary layer and δ is the boundary layer thickness. Also, Γ is assumed clockwise positive in the entire paper. Then, one can use the boundary layer theory along a curved surface (Goldstein 1938, pp. 119–120; Sears 1956) to write

$$\int_0^{\delta_1} \zeta u \, \mathrm{d}y = \int_0^{\delta_1} \left(\frac{\partial u}{\partial y} + \kappa u \right) u \, \mathrm{d}y = \frac{V_1^2}{2} + \frac{\Delta P_1}{\rho}, \tag{6.10}$$

where κ is the curvature of the wall. Writing an expression for the vorticity flux out of the boundary layer on the lower surface similar to (6.10) and substituting both in (6.9), one immediately arrives at the condition (6.8).

Setting $\Delta P_1 = \Delta P_2 = 0$ along with $V_{1,2} = U \pm (1/2)\gamma_{TE}$ as typically done in the classical theory of unsteady aerodynamics, the condition (6.8) results in

$$\dot{\Gamma}_{Kutta}(t) = -U\gamma_{TE}(t), \tag{6.11}$$

where γ_{TE} is the circulation distribution at the trailing edge (instantaneous strength of the shed vortex sheet per unit length at the shedding time). Equation (6.11) is equivalent to the classical Kutta condition ($P_1 = P_2$) and it is ubiquitously used in the classical theory of unsteady aerodynamics (Wagner 1925; Loewy 1957; Bisplinghoff *et al.* 1996, equations (5)–(318); Peters 2008, equation (11c); among others). Note that the main difference between the exact condition (6.8) and the classical Kutta condition (6.11) is two assumptions: (i) linearization ($V_{1,2} = U \pm (1/2)\gamma_{TE}$); and (ii) neglect of the viscous terms ΔP_1 and ΔP_2. The first assumption may be valid for small disturbance (small angle of attack). Using higher-fidelity computational simulations, we assess the validity of the second assumption. Figure 20 shows a comparison between the Kutta's rate of circulation development $\dot{\Gamma}_{Kutta}$ and the viscous contribution proportional to $\Delta P_{TE} = P_2 - P_1$, at different frequencies and Reynolds numbers. It is found that the viscous contribution $\dot{\Gamma}_{\Delta P}$ relative to the inviscid $\dot{\Gamma}_{Kutta}$ is not sensitive to frequency; it depends mainly on Reynolds number. This ratio is approximately 18 %, irrespective of the frequency k, at the lower Reynolds number $R = 10^4$ versus 6–7 % at $R = 10^5$. Moreover, a higher frequency, though it does not significantly affect the magnitude, causes a significant phase shift for the viscous contribution, which will in turn affect the phase of the total lift force at high frequencies.

In summary, the lower the Reynolds number, the larger is the viscous contribution to the bound circulation development relative to the inviscid one; and the higher the frequency, the larger is the phase shift of this viscous contribution. That is, at higher frequencies and lower Reynolds numbers, the viscous contribution to the bound circulation rate of development is of relatively larger magnitude and phase shift. This point, in addition to the wake viscous damping discussed above, may help to explain the physical reasons behind the additional phase lag in the lift response at high k and low R that could not be captured by the inviscid theory even at very small amplitudes. Since this viscous contribution is essentially neglected in the classical potential-flow framework by virtue of the classical Kutta condition (6.11), it is inferred that the Kutta condition is one of the reasons behind the inaccurate phase prediction of Theodorsen's lift frequency response function.

6.4. *Viscous reduction in virtual mass*

A closer look at the viscous correction B_v in (3.13) and its contribution to the circulatory lift in (4.10) implies that the viscous lift contribution is proportional to (in phase with) the 'effective' angle of attack

$$\alpha_{eff} = \frac{1}{U^2} \left[\frac{1}{2}a_0(t) + 2\sum_{n=1}^{\infty} na_n(t) \right]. \tag{6.12}$$

Note that this α_{eff} is different from the common notion of the effective angle of attack in potential flow. The former is a term special to the developed theory while
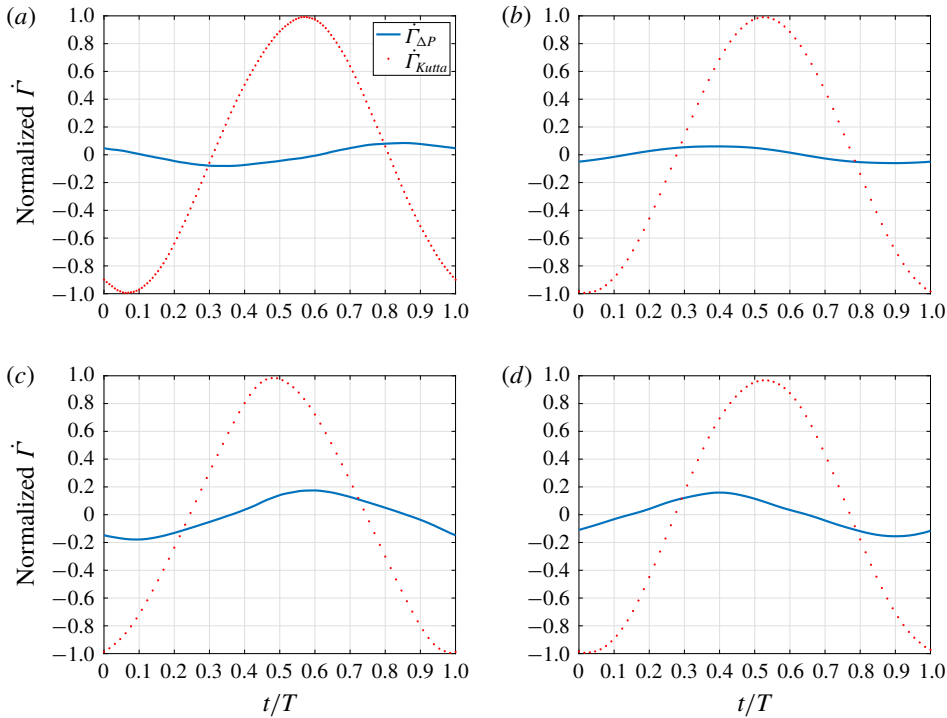
FIGURE 20. (Colour online) Inviscid and viscous contributions ($\dot{\Gamma}_{Kutta}$, $\dot{\Gamma}_{\Delta P}$) to the rate of bound circulation development over NACA 0012 undergoing a pitching oscillation about the quarter-chord point at different reduced frequencies and Reynolds numbers: (*a*) $R = 10^5$ and $k = 0.1$; (*b*) $R = 10^5$ and $k = 1$; (*c*) $R = 10^4$ and $k = 0.3$; (*d*) $R = 10^4$ and $k = 1$.

the latter is simply given by the angle of attack $\alpha_{3/4}$ at the three-quarter-chord point (Schlichting & Truckenbrodt 1979, p. 80). Equations (3.13) and (4.10) imply that the viscous contribution $\Delta_v C_L$ to the lift coefficient is simply proportional to α_{eff}:

$$\Delta_v C_L = -2\pi \tilde{B}_v(t) C(k) = 4\pi \epsilon^3 \lambda^{-5/4} B_e(\epsilon^{-1/2} \lambda^{-9/8} |\alpha_{eff}(t)|) \alpha_{eff}(t) C(k), \qquad (6.13)$$

where $B_e(\cdot)$ is a nonlinear function coming from the numerical solution of Chow & Melnik (1976) to the triple-deck problem, specifically from figure 3(*b*). This nonlinear function mainly affects the magnitude of $\tilde{B}_v$ with a weak effect on its phase, as shown in figures 21 and 22: the viscous contribution is in phase with α_{eff}.

Considering the studied case of a pitching flat plate about its quarter-chord point, the above definition of the effective angle of attack can be manipulated to write its Fourier transform as

$$\hat{\alpha}_{eff} = \hat{\alpha}_{3/4} C(k) - A_\alpha(3ik - 2k^2). \qquad (6.14)$$

Since the viscous contribution is proportional to α_{eff}, it is fair to write

$$\Delta_v C_L = A[\hat{\alpha}_{3/4} C(k) - A_\alpha(3ik - 2k^2)] C(k), \qquad (6.15)$$

where $A = 4\pi \epsilon^3 \lambda^{-5/4} B_e(\epsilon^{-1/2} \lambda^{-9/8} |\alpha_{eff}(t)|)$. Written this way, equation (6.15) shows how the viscous contribution induces more lag to the inviscid circulatory lift $\hat{\alpha}_{3/4} C(k)$:
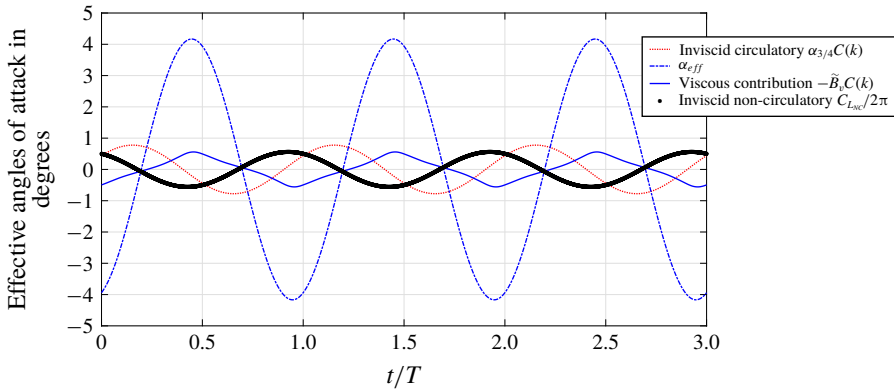
FIGURE 21. (Colour online) A comparison between the time history of the inviscid circulatory lift $\alpha_{3/4}C(k)$, the effective angle of attack α_{eff} for the developed viscous theory, the weighted effective angle of attack or the viscous contribution $-\tilde{B}_v C(k)$, and the inviscid added-mass lift. All lift coefficients are represented as effective angles of attack (i.e. normalized by 2π). Simulation of the developed viscous model is performed for a flat plate pitching about its quarter-chord point with amplitude $1°$ at $k = 1$ and $R = 10^4$. The viscous contribution $-\tilde{B}_v C(k)$ is opposite to the inviscid non-circulatory lift, decreasing the added-mass effect by 70%.

it provides a similar contribution ($\hat{\alpha}_{3/4}C(k)$) that is multiplied by $C(k)$ even further (i.e. possesses double the lag of Theodorsen's function). Also, A provides more lag because it depends algebraically on α_{eff}, which includes $C(k)$ in it (i.e. possesses lag).

Recalling the inviscid non-circulatory lift in this case,

$$\hat{C}_{L_{NC}} = \pi A_\alpha (ik - k^2/2), \tag{6.16}$$

equation (6.15) implies that the second component $-A_\alpha(3ik - 2k^2)$ of the viscous contribution is opposite to the non-circulatory lift (added mass). This fact is clearly seen in figures 21 and 22. Therefore, adding $\Delta_v C_L$ to the inviscid lift coefficient would decrease the added mass and cause a phase lag for its contribution.

It is noteworthy to comment on the results shown in figure 21 for a pitching flat plate about its quarter-chord point with amplitude $1°$ at $k = 1$ and $R = 10^4$. In addition to the points addressed above ($-\tilde{B}_v C(k)$ is in phase with α_{eff} and out of phase with $C_{L_{NC}}$), it is interesting to see the apparent nonlinear response of the viscous contribution even at this very small amplitude. Moreover, the phase lag between the inviscid circulatory lift and viscous contribution is very clear also in the Argand diagrams in figure 22. More importantly, the viscous contribution is as strong as the inviscid one at this low R and high k: its magnitude is 60% of the inviscid circulatory lift or 82% of the non-circulatory lift, which would have a significant effect on flutter (Bisplinghoff *et al.* 1996), if it happens at this low R and high k.

7. Conclusion

The triple-deck theory is a boundary layer theory developed in the 1970s to model local interactions in the vicinity of the trailing edge of an airfoil due to the discontinuity of the viscous boundary condition: from a zero slip on the airfoil to
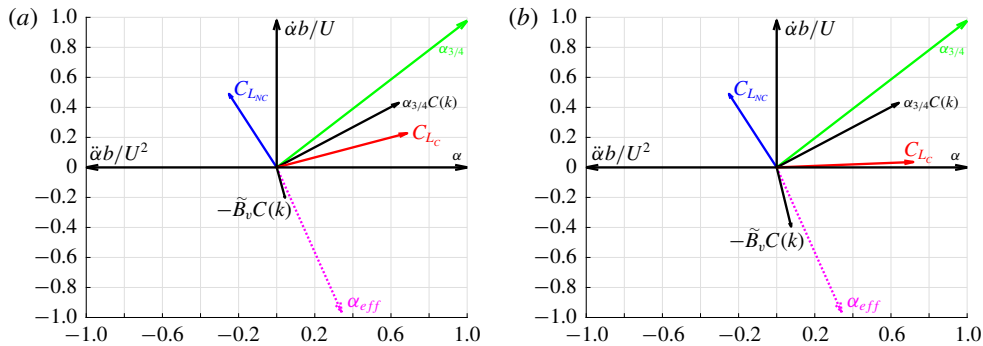
FIGURE 22. (Colour online) Argand diagram showing different components of lift for a pitching flat plate about its quarter-chord point at $k = 1$ and two different Reynolds numbers, (a) $R = 10^5$ and (b) $R = 10^4$. All lift coefficients are represented as effective angles of attack (i.e. normalized by 2π). The term α_{eff} is scaled down to one-quarter size to enhance visualization. The viscous contribution $\tilde{B}_v$ increases as R decreases, resulting in a larger phase difference between the inviscid circulatory contribution $\alpha_{3/4}C(k)$ and the total (viscous) circulatory component C_{L_c}, or a larger decrease in the added-mass effect.

a zero stress on the wake centreline. We utilized this theory to develop a viscous extension of the classical theory of unsteady aerodynamics, equivalently an unsteady extension of the viscous boundary layer theory. In particular, we developed an analytical model for the viscous unsteady lift response over a two-dimensional airfoil due to small-amplitude manoeuvres. The developed model admits airfoil flexibility (i.e. time-varying camber). The main modification to the classical thin airfoil theory is the introduction of a trailing-edge singularity term in the pressure distribution. The amplitude of such a correction cannot be obtained from potential flow. The Kutta condition dictates that it must vanish. We relaxed the Kutta condition and determined such a correction from pure viscous considerations: by drawing connections with the steady triple-deck theory.

Using the developed model, we constructed, for the first time, a theoretical viscous (Reynolds-number-dependent) extension of Theodorsen's lift frequency response. It was found that, as the Reynolds number decreases, the amplitude of the lift transfer function decreases. Also, that viscosity induces a significant lag to the lift dynamics is not captured by Theodorsen, particularly at higher reduced frequencies and lower Reynolds numbers. This finding was also supported by laminar simulations of Navier–Stokes equations on a sinusoidally pitching NACA 0012 at low Reynolds numbers and using Reynolds-averaged Navier–Stokes equations at relatively high Reynolds numbers. It was found that the viscosity-induced lag in the lift response can be interpreted as lag in the circulation development. This lag in the circulation dynamics was related to the Kutta condition via deriving an equation for the rate of change of circulation around the airfoil in terms of the pressure rise across the boundary layer at the trailing edge. It was concluded that the viscous contributions due to this pressure rise, which are typically neglected in a potential-flow analysis (employing the Kutta condition at the trailing edge), affect the magnitude of circulation development at lower Reynolds numbers and induce phase shift at higher frequencies. That is, the Kutta condition is one of the reasons behind the inaccurate phase prediction of Theodorsen's lift frequency response function.

From a different perspective, the viscous contribution to the unsteady lift was shown to significantly decrease the virtual mass at low Reynolds numbers and high frequencies. Recalling that both the unsteady phase lag of the circulatory lift and the virtual mass play crucial roles in determining the flutter boundary, these findings may shed some light on the reasons behind our meagre state of flutter predictability using potential flow; it is expected that the developed theory would enhance flutter prediction, particularly when occurring at high frequencies and low Reynolds numbers.

Acknowledgements

REFERENCES

ABRAMSON, H. N. & CHU, H.-H. 1959 A discussion of the flutter of submerged hydrofoils. *J. Ship Res.* **3** (2), 5–13.

ABRAMSON, H. N., CHU, W.-H & IRICK, J. T. 1967 Hydroelasticity with special reference to hydrofoil craft. *Tech. Rep.* 2557. NSRDC Hydromechanics Lab.

ABRAMSON, H. N. & RANSLEBEN, G. E. 1965 An experimental investigation of flutter of a fully submerged subcavitating hydrofoil. *J. Aircraft* **2** (5), 439–442.

ALBEN, S. 2008 The flapping-flag instability as a nonlinear eigenvalue problem. *Phys. Fluids* **20** (10), 104106.

ANSARI, S. A., ŻBIKOWSKI, R. & KNOWLES, K. 2006a Non-linear unsteady aerodynamic model for insect-like flapping wings in the hover. Part 1. Methodology and analysis. *Proc. Inst. Mech. Engrs* G **220** (2), 61–83.

ANSARI, S. A., ŻBIKOWSKI, R. & KNOWLES, K. 2006b Non-linear unsteady aerodynamic model for insect-like flapping wings in the hover. Part 2. Implementation and validation. *J. Aerospace Engng* **220**, 169–186.

BASS, R. L., JOHNSON, J. E. & UNRUH, J. F. 1982 Correlation of lift and boundary-layer activity on an oscillating lifting surface. *AIAA J.* **20** (8), 1051–1056.

BASU, B. C. & HANCOCK, G. J. 1978 The unsteady motion of a two-dimensional aerofoil in incompressible inviscid flow. *J. Fluid Mech.* **87** (01), 159–178.

BATCHELOR, G. K. 2000 *An Introduction to Fluid Dynamics*. Cambridge University Press.

BIRKHOFF, G. 1962 *Helmholtz and Taylor Instability*, *(Proc. Symp. Applied Mathematics)*, vol. 13, pp. 55–76. American Mathematical Society.

BIRNBAUM, W. 1924 Der Schlagflugelpropeller und die kleinen Schwingungen elastisch befestigter Tragfluegel. *Z. Flugtech. Motorluftschiffahrt* **15**, 128–134.

BIRNBAUM, W. & ACKERMANN, W. 1923 Die tragende Wirbelfläche als Hilfsmittel zur Behandlung des ebenen Problems der Tragflügeltheorie. *Z. Angew. Math. Mech.* **3** (4), 290–297.

BISPLINGHOFF, R. L., ASHLEY, H. & HALFMAN, R. L. 1996 *Aeroelasticity*. Dover Publications.

BLASIUS, H. 1908 *Grenzschichten in Flüssigkeiten mit kleiner Reibung*. B.G. Teubner.

BROWN, S. N. & CHENG, H. K. 1981 Correlated unsteady and steady laminar trailing-edge flows. *J. Fluid Mech.* **108**, 171–183.

BROWN, S. N. & DANIELS, P. G. 1975 On the viscous flow about the trailing edge of a rapidly oscillating plate. *J. Fluid Mech.* **67** (04), 743–761.

BROWN, S. N. & STEWARTSON, K. 1970 Trailing-edge stall. *J. Fluid Mech.* **42** (03), 561–584.

CHOW, R. & MELNIK, R. E. 1976 Numerical solutions of the triple-deck equations for laminar trailing-edge stall. In *Proceedings of the 5th International Conference on Numerical Methods in Fluid Dynamics June 28–July 2 1976, Twente University, Enschede*, pp. 135–144. Springer.

CHU, W.-H. 1961 An aerodynamic analysis for flutter in Oseen-type viscous flow. *J. Aero. Sci.* **29**, 781–789.

CHU, W.-H. & ABRAMSON, H. N. 1959 An alternative formulation of the problem of flutter in real fluids. *J. Aero. Sci.* **26** (10), 683–684.

CRIGHTON, D. G. 1985 The Kutta condition in unsteady flow. *Annu. Rev. Fluid Mech.* **17** (1), 411–445.

DANIELS, P. G. 1978 On the unsteady Kutta condition. *Q. J. Mech. Appl. Maths* **31** (1), 49–75.

DING, Q. N. & WANG, D.-L. 2006 The flutter of an airfoil with cubic structural and aerodynamic non-linearities. *Aerosp. Sci. Technol.* **10** (5), 427–434.

GARRICK, I. E. 1937 Propulsion of a flapping and oscillating airfoil. *Tech. Rep.* NACA-TR-567.

GARRICK, I. E. 1938 On some reciprocal relations in the theory of nonstationary flows. *NACA Tech. Rep.* 629.

GLAUERT, H. 1926 *The Elements of Aerofoil and Airscrew Theory*. Cambridge University Press.

GOLDSTEIN, S. 1930 Concerning some solutions of the boundary layer equations in hydrodynamics. *Math. Proc. Camb. Phil. Soc.* **26** (1), 1–30.

GOLDSTEIN, S. 1938 *Modern Developments in Fluid Dynamics: An Account of Theory and Experiment Relating to Boundary Layers, Turbulent Motion and Wakes*. Clarendon Press.

GRAFTIEAUX, L., MICHARD, M. & GROSJEAN, N. 2001 Combining PIV, POD and vortex identification algorithms for the study of unsteady turbulent swirling flows. *Meas. Sci. Technol.* **12** (9), 1422–1429.

HEMATI, M. S., ELDREDGE, J. D. & SPEYER, J. L. 2014 Improving vortex models via optimal control theory. *J. Fluids Struct.* **49**, 91–111.

HENRY, C. J. 1961 Hydrofoil flutter phenomenon and airfoil flutter theory. *Tech. Rep.* 856. Davidson Laboratory.

HOWARTH, L. 1935 The theoretical determination of the lift coefficient for a thin elliptic cylinder. *Proc. R. Soc. Lond.* A **149** (868), 558–586.

HUSSEIN, A. A. & CANFIELD, R. A. 2017 Unsteady aerodynamic stabilization of the dynamics of hingeless rotor blades in hover. *AIAA J.* **56** (3), 1298–1303.

HUSSEIN, A. A., TAHA, H., RAGAB, S. & HAJJ, M. R. 2018 A variational approach for the dynamics of unsteady point vortices. *Aerosp. Sci. Technol.* **78**, 559–568.

JOBE, C. E. & BURGGRAF, O. R. 1974 The numerical solution of the asymptotic equations of trailing edge flow. *Proc. R. Soc. Lond.* A **340** (1620), 91–111.

JONES, M. A. 2003 The separated flow of an inviscid fluid around a moving flat plate. *J. Fluid Mech.* **496**, 405–441.

JOUKOWSKY, N. 1910 Über die konturen der Tragflächen der Drachenflieger. *Z. Flugtech. Motorluftschiffahrt* **1**, 281–284.

KATZ, J. & PLOTKIN, A. 2001 *Low-Speed Aerodynamics*. Cambridge University Press.

KRYLOV, N. M. & BOGOLIUBOV, N. N. 1943 *Introduction to Non-Linear Mechanics. (AM-11)*. Princeton University Press.

KÜSSNER, H. G. 1929 Schwingungen von Flugzeugflügeln. *Jahrbuch der deutscher Versuchsanstalt für Luftfahrt especially Section E3 Einfluss der Baustoff-Dämpfung*, pp. 319–320.

KUTTA, W. M. 1902 Auftriebskräfte in strömenden Flüssigkeiten. *Illustrierte Aeronautische Mitteilungen* **6** (133), 133–135.

LAMB, H. 1932 *Hydrodynamics*. Cambridge University Press.

LANGLOIS, W. E. & DEVILLE, M. O. 2014 *Slow Viscous Flow*. Springer.

LI, J. & WU, Z.-N. 2015 Unsteady lift for the Wagner problem in the presence of additional leading/trailing edge vortices. *J. Fluid Mech.* **769**, 182–217.

LIBRESCU, L., CHIOCCHIA, G. & MARZOCCA, P. 2003 Implications of cubic physical/aerodynamic non-linearities on the character of the flutter instability boundary. *Intl J. Non-Linear Mech.* **38** (2), 173–199.

LIGHTHILL, M. J. 1953 On boundary layers and upstream influence. II. Supersonic flows without separation. *Proc. R. Soc. Lond.* A **217** (1131), 478–507.

LOEWY, R. G. 1957 A two-dimensional approximation to unsteady aerodynamics in rotary wings. *J. Aero. Sci.* **24**, 81–92.

MANDRE, S. & MAHADEVAN, L. 2010 A generalized theory of viscous and inviscid flutter. *Proc. R. Soc. Lond.* A **466** (2113), 141–156.

MENTER, F. R. 1994 Two-equation eddy-viscosity turbulence models for engineering applications. *AIAA J.* **32** (8), 1598–1605.

MESSITER, A. F. 1970 Boundary-layer flow near the trailing edge of a flat plate. *SIAM J. Appl. Maths* **18** (1), 241–257.

MESSITER, A. F. 1983 Boundary-layer interaction theory. *Trans. ASME J. Appl. Mech.* **50** (4b), 1104–1113.

MICHELIN, S. & SMITH, S. G. L. 2009 An unsteady point vortex method for coupled fluid–solid problems. *Theor. Comput. Fluid Dyn.* **23** (2), 127–153.

MULTHOPP, H. 1950 *Methods for Calculating the Lift Distribution of Wings (Subsonic Lifting-Surface Theory)*. Aeronautical Research Council.

OGATA, K. & YANG, Y. 1970 *Modern Control Engineering*. Prentice-Hall.

ORSZAG, S. A. & CROW, S. C. 1970 Instability of a vortex sheet leaving a semi-infinite plate. *Stud. Appl. Maths* **49** (2), 167–181.

PETERS, D. A. 2008 Two-dimensional incompressible unsteady airfoil theory – an overview. *J. Fluids Struct.* **24**, 295–312.

PITT FORD, C. W. & BABINSKY, H. 2013 Lift and the leading-edge vortex. *J. Fluid Mech.* **720**, 280–313.

PRANDTL, L. 1918 *Gesammelte Abhandlungen zur angewandten Mechanik, Hydro-und Aerodynamik*. Springer.

PRANDTL, L. 1924 Über die Entstehung von Wirbeln in der idealen Flüssigkeit, mit Anwendung auf die Tragflügeltheorie und andere Aufgaben. In *Vorträge aus dem Gebiete der Hydro-und Aerodynamik (Innsbruck 1922)*, pp. 18–33. Springer.

PRESTON, J. H. 1943 *The Approximate Calculation of the Lift of Symmetrical Aerofoils taking Account of the Boundary Layer, with Application to Control Problems*. HM Stationery Office.

PULLIN, D. I. & WANG, Z. 2004 Unsteady forces on an accelerating plate and application to hovering insect flight. *J. Fluid Mech.* **509**, 1–21.

RAMESH, K., GOPALARATHNAM, A., EDWARDS, J. R., OL, M. V. & GRANLUND, K. 2013 An unsteady airfoil theory applied to pitching motions validated against experiment and computation. *Theor. Comput. Fluid Dyn.* **27**, 1–22.

RAMESH, K., GOPALARATHNAM, A., GRANLUND, K., OL, M. V. & EDWARDS, J. R. 2014 Discrete-vortex method with novel shedding criterion for unsteady aerofoil flows with intermittent leading-edge vortex shedding. *J. Fluid Mech.* **751**, 500–538.

REZAEI, A. S. & TAHA, H. 2017 Computational study of lift frequency responses of pitching airfoils at low Reynolds numbers. AIAA-Paper 2017-0716.

ROBINSON, A. & LAURMANN, J. A. 1956 *Wing Theory*. Cambridge University Press.

ROTT, N. 1956 Diffraction of a weak shock with vortex generation. *J. Fluid Mech.* **1** (01), 111–128.

ROTT, N. & GEORGE, M. B. T. 1955 An approach to the flutter problem in real fluids. *Tech. Rep.* 509.

SATYANARAYANA, B. & DAVIS, S. 1978 Experimental studies of unsteady trailing-edge conditions. *AIAA J.* **16** (2), 125–129.

SAVAGE, S. B., NEWMAN, B. G. & WONG, D. T.-M. 1979 The role of vortices and unsteady effects during the hovering flight of dragonflies. *J. Expl Biol.* **83** (1), 59–77.

SCHLICHTING, H. & TRUCKENBRODT, E. 1979 *Aerodynamics of the Airplane*. McGraw-Hill.

SEARS, W. R. 1956 Some recent developments in airfoil theory. *J. Aero. Sci.* **23**, 490–499.

SEARS, W. R. 1976 Unsteady motion of airfoils with boundary-layer separation. *AIAA J.* **14** (2), 216–220.

SHEN, S. F. & CRIMI, P. 1965 The theory for an oscillating thin airfoil as derived from the Oseen equations. *J. Fluid Mech.* **23** (03), 585–609.

SMITH, F. T. 1983 Interacting flow theory and trailing edge separation – no stall. *J. Fluid Mech.* **131**, 219–249.

SPENCE, D. A. 1954 Prediction of the characteristics of two-dimensional airfoils. *J. Aero. Sci.* **21**, 577–587.

STEWARTSON, K. 1968 On the flow near the trailing edge of a flat plate. *Proc. R. Soc. Lond.* A **306** (1486), 275–290.

STEWARTSON, K. 1974 Multistructured boundary layers on flat plates and related bodies. *Adv. Appl. Mech.* **14** (145–239), 136.

STEWARTSON, K. 1981 D'Alembert's paradox. *SIAM Rev.* **23** (3), 308–343.

TAHA, H., HAJJ, M. R. & BERAN, P. S. 2014 State space representation of the unsteady aerodynamics of flapping flight. *Aerosp. Sci. Technol.* **34**, 1–11.

TCHIEU, A. A. & LEONARD, A. 2011 A discrete-vortex model for the arbitrary motion of a thin airfoil with fluidic control. *J. Fluids Struct.* **27** (5), 680–693.

THEODORSEN, T. 1935 General theory of aerodynamic instability and the mechanism of flutter *NACA Tech. Rep.* 496.

TIETJENS, O. K. G. & PRANDTL, L. 1934 *Applied Hydro- and Aeromechanics: Based on Lectures of L. Prandtl.* Courier Corporation.

TRUCKENBRODT, E. 1953 Tragflächentheorie bei inkompressibler Strömung. *Jahrbuch*, pp. 40–65.

VELDMANN, A. E. P. & VAN DE VOOREN, A. I. 1975 Drag of a finite plate. In *Proceedings of the Fourth International Conference on Numerical Methods in Fluid Dynamics*, pp. 423–430. Springer.

VON KARMAN, T. & SEARS, W. R. 1938 Airfoil theory for non-uniform motion. *J. Aero. Sci.* **5** (10), 379–390.

WAGNER, H. 1925 Uber die Entstehung des dynamischen Auftriebs von Tragflugeln. *Z. Angew. Math. Mech.* **5**, 17–35.

WANG, C. & ELDREDGE, J. D. 2013 Low-order phenomenological modeling of leading-edge vortex formation. *Theor. Comput. Fluid Dyn.* **27** (5), 577–598.

WEISSINGER, J. 1949 Über eine erweiterung der prandtlschen theorie der tragenden linie. *Math. Nachrichten* **2** (1–2), 45–106.

WILCOX, D. C. 1998 *Turbulence Modeling for CFD.* DCW Industries.

WOOLSTON, D. S. & CASTILE, G. E. 1951 Some effects of variations in several parameters including fluid density on the flutter speed of light uniform cantilever wings. *NACA Tech. Rep.* 2558.

XIA, X. & MOHSENI, K. 2017 Unsteady aerodynamics and vortex-sheet formation of a two-dimensional airfoil. *J. Fluid Mech.* **830**, 439–478.

YAN, Z., TAHA, H. & HAJJ, M. R. 2014 Geometrically-exact unsteady model for airfoils undergoing large amplitude maneuvers. *Aerosp. Sci. Technol.* **39**, 293–306.

YONGLIANG, Y., BINGGANG, T. & HUIYANG, M. 2003 An analytic approach to theoretical modeling of highly unsteady viscous flow excited by wing flapping in small insects. *Acta Mechanica Sin.* **19** (6), 508–516.

ZAKARIA, M. Y., AL-HAIK, M. Y. & HAJJ, M. R. 2015 Experimental analysis of energy harvesting from self-induced flutter of a composite beam. *Appl. Phys. Lett.* **107** (2), 023901.

ZAKARIA, M. Y., TAHA, H. & HAJJ, M. R. 2017 Measurement and modeling of lift enhancement on plunging airfoils: a frequency response approach. *J. Fluids Struct.* **69**, 187–208.